Article

Amazon carbon emissions driven by human actions amplified by droughts

https://doi.org/10.1038/s41586-026-11168-1

Received: 7 November 2025

Accepted: 15 September 2026

Published online: 21 October 2026

Open access

Check for updates

Luciana V. Gatti[1,2]✉, Camilla L. Cunha[1], Juan C. G. Blas[1], A. Scott Denning[3], Mariane S. Reis[1], Luciano Marani[1], Egidio Arai[1], Cassiano Gustavo Messias[1], Dhemerson E. Conciani[4], John B. Miller[5], Vanúcia Schumacher[1], Kleber P. Naccarato[1], Jose Marengo[6], Ane A. C. Alencar[4], Luciana Soler[1], Claudio Almeida[1], Lucas Gatti Domingues[2], Caio S. C. Correia[1], Raiane A. L. Neves[1], Carlos Nobre[7], Sergio M. Corrêa[8], Elliott Campbell[9], Jennifer E. Johnson[10], Joseph A. Berry[11], Alber H. Sanchez[1], Francine M. da Silva[1], Vagner L. Camilotti[1], Christiane Silvestrini[1], Filipe Loyola Lopes[1], Xin Lan[5], Gabrielle Pétron[5], Marcio Malacarne[1] & Guilherme B. M. Machado[1]

The Amazon carbon sink is weakening as deforestation[1–5], rising tree mortality[6–8] and climate change disrupt the climatic conditions that sustain a humid tropical forest[9–11]. Forest loss reduces precipitation, increases temperatures and lengthens the dry season, driving higher carbon emissions[1–4,11,12]. Climate stress is stronger in more deforested regions, rendering forests progressively more flammable[1,9,13]. Large-scale climate events, such as El Niño, further amplify regional climate impacts[9,14–17]. Here we present an analysis of 15 years of Amazonian carbon fluxes derived from atmospheric CO_2 measurements. We determine a carbon balance of 0.32 ± 0.08 PgC yr^{-1}, with fires acting as the dominant source (0.40 ± 0.07 PgC yr^{-1}) and forest uptake becoming increasingly unable to offset emissions. Furthermore, we investigate key drivers of the carbon emissions of Amazonia and identify three distinct year groups. Group 1 (2011–2014, 2017 and 2018) represents the role of the Amazon in the global carbon balance (0.11 ± 0.08 PgC yr^{-1}) during wetter years with low human activity, such as deforestation, biomass burning and degradation. Group 2 (2019–2022) represents Amazon carbon emissions (0.43 ± 0.13 PgC yr^{-1}) from human activities (mainly deforestation and degradation) during years with low climatic stress. Group 3 (2010, 2015, 2016, 2023 and 2024) has the highest carbon emissions (0.49 ± 0.07 PgC yr^{-1}) and comprises warm and dry years (high climate stress), such as El Niño and the warming of the Tropical North Atlantic Ocean, associated with biomass burning.

Amazonia, the largest tropical forest in the world, has lost substantial carbon stocks due to large-scale deforestation and other land-use changes. Remaining forests in the region have offset some of this carbon loss through carbon sequestration processes. However, this capacity is declining, primarily because of increased tree mortality[6–8,18] and changes in regional climatic conditions modified by deforestation[1,3,9,13]. The Amazon forest stores approximately 123 ± 23 billion tonnes of carbon (PgC) in vegetation and soils[19,20]. The interactions among the forest ecosystem, hydrological cycle and regional climate are complex, with atmospheric moisture recycling by evapotranspiration accounting for up to half of precipitation[16]. Direct human activities within Amazonia, including deforestation, forest degradation and biomass burning, have profoundly altered the carbon balance of the region and climate[11]. Forest loss reduces precipitation, raises temperatures and lengthens the dry season, delaying the onset of the wet season[1,3,4,14,16]. During periods of extreme climatic variability, such as El Niño or anomalously high Tropical North Atlantic (TNA) sea-surface temperatures (SSTs), these impacts are amplified through the interaction of accumulated forest loss, global warming, changing circulation and large-scale anomalies[9,14,16].

Many questions remain about the main drivers of carbon emissions and variability in Amazonia. Studies based on modelling and bottom-up techniques show increased emissions during extreme climate (warm and dry) years, pointing to extreme events as the reason for increased carbon emissions. However, our direct atmospheric measurements show a more complex situation. Here, we use our 15-year history of Amazonian carbon fluxes derived from atmospheric CO_2 measurements to answer important questions about the main factors driving increased carbon emissions and variability in the Amazon and whether they are caused by global extreme climate events or direct human activities (deforestation, biomass burning and degradation) in the Amazon.

[1]General Coordination of Earth Science (CGCT), National Institute for Space Research (INPE), São Paulo, Brazil. [2]Nuclear and Energy Research Institute (IPEN), São Paulo, Brazil. [3]Yale University, New Haven, CT, USA. [4]Amazon Environmental Research Institute (IPAM), Brasilia, Brazil. [5]National Oceanic and Atmospheric Administration (NOAA), Boulder, CO, USA. [6]CEMADEN, São Paulo, Brazil. [7]Institute of Advanced Studies, University of São Paulo, São Paulo, Brazil. [8]Rio de Janeiro State University (UERJ), Rio de Janeiro, Brazil. [9]Environmental Studies Department, University of California, Santa Cruz, Santa Cruz, CA, USA. [10]University of Kansas, Lawrence, KS, USA. [11]Department of Global Ecology, Carnegie Institution for Science, Stanford, CA, USA. ✉e-mail: lvgatti@gmail.com

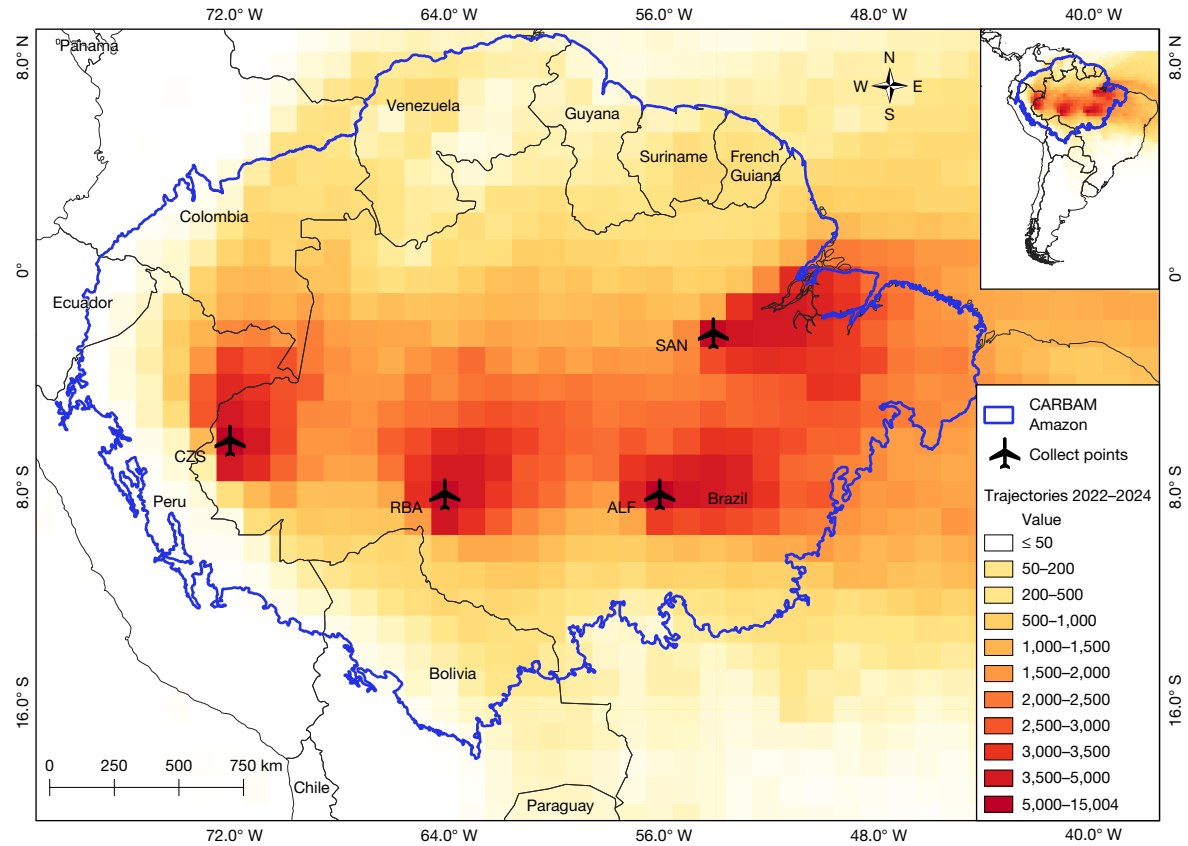


Fig. 1 | Aircraft sampling region of influence. Annual mean regions of influence, integrating RBA, ALF, SAN and CZS sites, based on back-trajectory density along the years 2022–2024, calculated by the HYSPLIT trajectory model for each flask (sample height). The blue line corresponds to Amazonia area of 6.7×10^6 km^2 adopted in this study (Methods). The regions of influence based on these four sites correspond to 95% of Amazonia. The regions of influence for the periods 2010–2012 and 2013–2021, as well as for each site, are presented in Extended Data Fig. 2.

Historic land use change

In 2000, deforestation in the Brazilian Amazon represented a total area of 474,770 km^2 (12.5% of the Brazilian Amazon, 3.8×10^6 km^2). The Brazilian Amazon represents 58% of the Pan-Amazonia region (Fig. 1). By 2004, the PRODES programme[21] of Brazil for monitoring native vegetation had recorded cumulative deforestation of 612,225 km^2 across the Legal Amazon, equivalent to 15.5% of the original forest cover of the region. Between 2004 and 2012, the annual rate of deforestation fell 84% as a result of public policies designed to curb clearing[22,23], reaching a cumulative loss of 697,319 km^2 (18.4% of the total forest area). The rate began to rise again from 2013 to 2018, when total forest loss reached 19.5%, and accelerated sharply after 2019, reaching 791,835 km^2 (20.9%) in 2022. Although the annual rate of deforestation declined strongly in 2023 and 2024 (30% and 47%, respectively) relative to the 2019–2022 period, cumulative forest loss still reached 807,301 km^2 (21.3%). From 2010 to 2024, pasture area expanded by 19%, soybean plantation area by 193% and mining by 272% (ref. 24) to estimated values of 561,416 km^2, 59,368 km^2 and 3,956 km^2, respectively (Supplementary Fig. 1).

Amazon precipitation and temperature changes

We present precipitation and temperature time series from 1979 to 2024 in Extended Data Fig. 1. To assess the impact of the past six years, during which deforestation accelerated sharply between 2019 and 2022, on precipitation and temperature, we compared the previously studied period[1] (1979–2018) with the current period from 1979 to 2024, using the same database for both periods (Methods). From 1979 to 2018, the changes in annual precipitation were not statistically significant (27 ± 69 mm); however, from 1979 to 2024, there was a reduction of 174 ± 69 mm, representing an 8% decrease. During the dry-season peak period (August–October), from 1979 to 2018, precipitation decreased by 17% (64 ± 19 mm), and from 1979 to 2024, by 20% (83 ± 18 mm). The increase in annual temperature from 1979 to 2018 was 0.93 ± 0.13 °C, and from 1979 to 2024 was 1.13 ± 0.13 °C, representing a 0.20 °C increase over 6 years. During the dry-season peak period, the increase in temperature was 1.51 ± 0.17 °C from 1979 to 2018 and 1.81 ± 0.18 °C from 1979 to 2024, representing a 0.30 °C increase over 6 years. Between 2018 and 2024, Amazonia lost an additional 60,964 km^2 of primary forest and 564,532 km^2 of burned area, representing a significant increase in human activity impacting the region since 2019. Further discussion of changes in climatic conditions in Amazonia and the studied regions is provided in Extended Data Fig. 1, Extended Data Table 1 and Supplementary Discussion 1.

Regional analyses show that the most pronounced temperature increase occurred in the southeast region (ALF), with warming of 2.19 ± 0.21 °C during the dry-season peak and 1.37 ± 0.15 °C in the annual mean between 1979 and 2024. From 2018 to 2024, this region lost 37,930 km^2 (62% of the total deforestation of the Brazilian Amazon) of primary forest. The most intense decline in precipitation happened in the northeast region (SAN). From 1979 to 2024, annual precipitation decreased by 304 ± 150 mm (12%), and during the dry-season peak, it declined by 37% (77 ± 23 mm). Over the same six-year period, SAN lost 15,023 km^2 (25% of the total deforestation) of primary forest. More details are presented in Extended Data Fig. 1, Extended Data Table 1 and Supplementary Discussion 3.

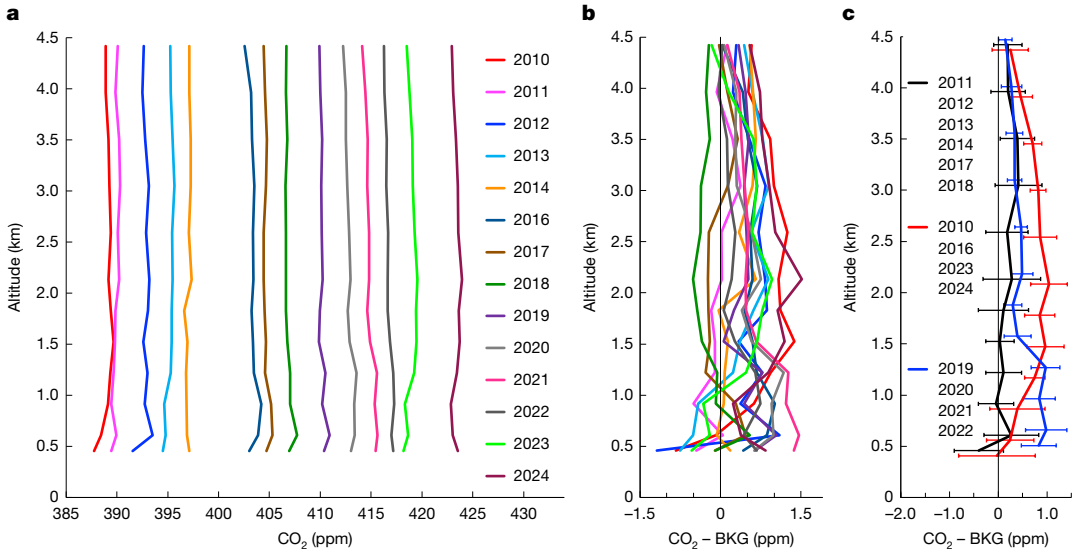


Fig. 2 | Amazon annual mean vertical profile. a, Amazon CO_2 annual mean mole fraction (micromole of CO_2 per mole dry air, or ppm) by height and by year. **b**, Same as **a**, but differenced from the CO_2 background (BKG). **c**, Same as **b**, but multi-year means grouped according to statistical analysis of the years (group 1 of wet years and low human activities; group 2 of years with high human activities and low climatic stress; group 3 of dry and warm years and associated biomass burning) (Methods). The bars represent the standard deviation of the mean for the year.

Annual mean vertical profiles

This study includes 1,017 vertical profiles conducted between 2010 and 2024 at four Amazonian sites, whose upwind areas of influence represent nearly the entirety of Amazonia (Fig. 1 and Extended Data Fig. 2). Vertical profiles were typically performed twice per month, from 4.4 km above sea level (a.s.l.) to near the surface (about 0.3 km a.s.l.), sampling air at 12 heights in a descending helical trajectory at each of the four sites between 12:00 and 13:00 local time. Air samples were analysed for CO_2 and CO at the Greenhouse Gas Laboratory (LaGEE/INPE), São José dos Campos, Brazil. The Amazon exhibits a dominant lower-tropospheric circulation pattern, with air masses originating over the tropical Atlantic Ocean, crossing the Amazon towards the Andes, then to the southern regions, and returning to the Atlantic in the southern regions. This circulation enables integration of both natural and anthropogenic processes by computing atmospheric mass balance across vertical profiles of sites. Here, we present Amazonian annual mean CO_2 vertical profiles (VP; Fig. 2a), and the profiles differenced from the CO_2 background (ΔVP; Fig. 2b) for 2010–2024, calculated from the annual mean profiles at each site (Extended Data Fig. 3), using the same weighting methodology used for Amazonia carbon balance calculations[1,13] (Methods). Most years show a positive ΔVP near the surface (Fig. 2b), indicating that Amazonia is a net carbon source rather than a sink and cannot offset regional anthropogenic emissions.

Carbon flux from column budget technique

Carbon fluxes were calculated using the atmospheric column budget technique[1] for each vertical profile and site over a 15-year study period. Total carbon flux (TCF), fire carbon flux (FCF) and net biome exchange (NBE) monthly mean carbon fluxes (TCF subtracted by FCF = NBE) for each site were derived from the two vertical profiles collected per month, and Amazonia-wide monthly and annual mean fluxes were computed using a weighted mean approach that accounts for regional contributions[1,13] (Methods). Figure 3 shows the Amazon carbon balance over 15 years, alongside some climatic and anthropogenic drivers. Examining the annual mean vertical profiles (Fig. 2) and the annual carbon balance (Fig. 3, blue bars) shows strong variability over the 15-year period.

Results and discussion of grouping of years

To better understand the variability in Amazonia annual carbon balance, we use *k*-means clustering analysis to group years, taking into account the following parameters: annual carbon balance (TCF), precipitation, temperature, deforestation (annual increment and accumulated), burned area (integrating all vegetation types)[25], fire spots, Oceanic Niño Index[26] (ONI) and TNA warming[27]. The cluster analysis identified the 15 years as belonging to three clusters: group 1 (2011, 2012, 2013, 2014, 2017 and 2018); group 2 (2019, 2020, 2021 and 2022); and group 3 (2010, 2015, 2016, 2023 and 2024). See the statistical analysis in Methods, Extended Data Fig. 4, Extended Data Tables 2 and 3, Supplementary Discussion 2 and Supplementary Table 1. Group 1 is characterized by wetter years and low human activities. Group 2 reflects a period with intense human activity—deforestation and degradation (biomass-burning, selective logging, mining and edge effects), and low climatic stress. Group 3 comprises years characterized by intense global climate events, such as El Niño and TNA events with associated biomass burning.

Group 1 (Fig. 2c, Extended Data Table 3a and Extended Data Fig. 5), representing the wettest years with low levels of human disturbance (deforestation and degradation), shows a near-neutral annual mean total carbon flux (TCF) of 0.11 ± 0.08 PgC yr^{-1} and ΔVP (VP − BKG) of 0.14 ppm, resulting from a carbon sink (−0.20 ± 0.12 PgC yr^{-1}) that offsets 64% of fire emissions (0.32 ± 0.07 PgC yr^{-1}). The annual deforestation and burned area were 6,389 km^2 and 55,115 km^2, respectively. This result indicates that Amazonia did not significantly contribute to the global carbon balance during wet years and with low human disturbance.

Group 2 years (Figs. 2c and 3, Extended Data Table 3b and Extended Data Fig. 5) were characterized by a period with higher levels of human disturbance and weak governance[13]. During this period, the annual deforestation rate rose by 97%, whereas the burned area increased by 25%, resulting in a TCF of 0.43 ± 0.09 PgC yr^{-1} and a ΔVP of 0.53 ppm, representing increases of 291% and 379% relative to group 1, respectively. The annual mean temperature was the same as in group 1, and precipitation was 134 mm (6%) lower (mainly due to the 2020 wet season), indicating low climatic stress during this period. In August 2020, a strong and prolonged La Niña event began and lasted until February 2023 (Fig. 4). During this period, carbon uptake gradually increased in

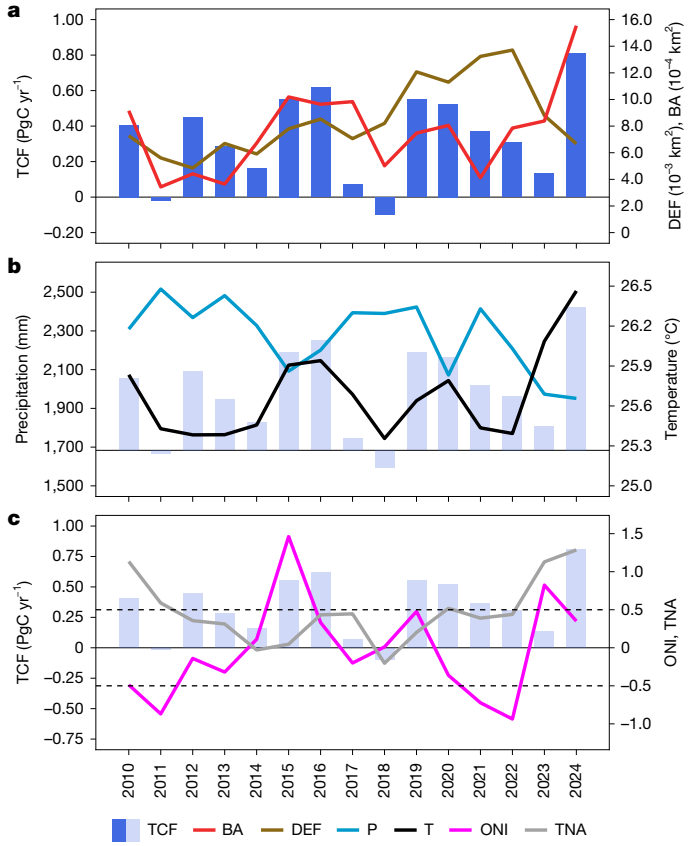


Fig. 3 | Amazon carbon balance and its drivers. a, Amazon annual mean TCF (blue bars, repeated as translucent blue bars in **b** and **c**), annual deforestation (DEF) from PRODES[21] (brown line) and total burned area (BA) integrating all vegetation types[25] (red line). **b**, Annual mean precipitation (cyan line) and annual mean temperature (black line). **c**, Annual mean ONI (pink line) and annual mean TNA index (grey line). The positive dashed line indicates years with values exceeding 0.5, corresponding to extreme El Niño and TNA events (Methods).

the first quarter of each year (Fig. 4), offsetting an ever-greater proportion of anthropogenic emissions. As climate stress was very low during this period, it mainly represents the carbon emissions from human activity in Amazonia.

Group 3 (Extended Data Table 3c and Extended Data Fig. 5) comprises years characterized by intense global climate events, such as El Niño and TNA warming. The mean ONI and TNA values for group 3 were higher than those for groups 1 and 2. Any years from groups 1 and 2 presented El Niño and/or warming TNA events. The El Niño events occurred in 2015–2016 (strong–very strong) and 2023 (strong; Fig. 3c), and the warming TNA events occurred in 2010 (moderate) and 2023–2024 (moderate–strong). We used the same ONI classification criterion[28] for the TNA events (Methods). We also observed in Fig. 2c that the group 3 vertical profile showed an increase in the free-troposphere layer, unlike the other two; this is due to convective transport induced by the fire. Both El Niño and TNA warming contribute to reduced precipitation and increased temperatures in Amazonia. On average, group 3 received 308 mm (13%) less annual precipitation than group 1, with 20% less during the wet-season peak (January–March), and 17% less during the dry-season peak (August–October). The annual mean, wet-season peak and dry-season peak temperatures were higher than those of group 1 by 0.5 °C, 0.4 °C and 0.8 °C, respectively. These drought and warming conditions in Amazonia increased the flammability of the forest. We observed a 92% increase in burned area[25] compared with group 1, whereas deforestation[21] was 22% higher. TCF was 0.49 ± 0.07 PgC y^{-1}, and ΔVP was 0.61 ppm, both of which were 325% higher than Group 1. However, for this group, NBE was −0.06 ± 0.10 PgC y^{-1} (nearly neutral sink), indicating that the main source of carbon is not the forest itself, but, again, human influence that promotes fires. Furthermore, recent climatic conditions interfere with the consequences of an intense El Niño year on the forest, as can be observed in 2023 and 2024 (Extended Data Tables 2 and 3 and Extended Data Fig. 7). FCF was 0.55 ± 0.10 PgC yr^{-1}, 72% higher than group 1 and 53% higher than group 2, showing that fire emissions are an important characteristic of group 3. This finding highlighted the importance of clarifying the origin of fires, whether natural or anthropogenic. Therefore, a study was conducted to identify the relationship between lightning and forest fires in group 3. During the years of this group, it was found that lightning-induced ignition for fire events represented 1.6% and 1.0%, respectively, for the years 2023 and 2024 (Methods and Extended Data Fig. 6), allowing us to conclude that the emissions from group 3 originated primarily from human-induced fires, which were amplified by drought conditions. The years 2023 and 2024 were chosen to ensure gathering a more accurate cloud-to-ground lightning dataset, as higher-quality and more reliable data are only available from 2017 onwards.

These findings underscore the dominant role of direct human disturbance in Amazonia (Fig. 5, a schematic grouping summary), driving year-to-year changes in carbon fluxes and highlighting the urgent need for mitigation to prevent the approach of the region to a climatic tipping point[29,30]. Climatic stress amplifies the effects of human-induced fire, because drought conditions substantially increase forest flammability[1,9–11,13,15,31–33].

The exceptional years 2023 and 2024

The 2023 wet season exhibited the largest carbon sink over our study period of 15 years (Fig. 4 and Extended Data Fig. 7), which occurred after three consecutive La Niña years (Fig. 4). The 2023 Amazonia carbon balance was similar to that of group 1 (0.11 ± 0.09 PgC yr^{-1}), because the wet-season sink offset 75% of the carbon emissions from deforestation

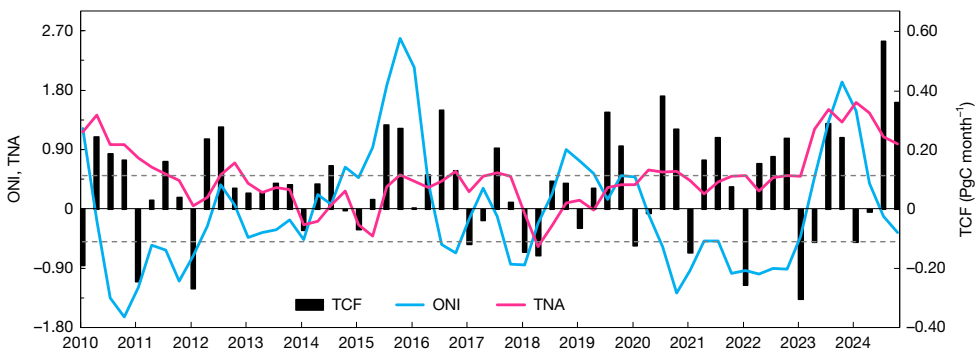


Fig. 4 | Quarterly Amazon carbon flux, ONI and TNA index. Quarterly mean TCF (black bars), ONI (cyan line)[26] and TNA index (pink line)[27] of Amazon. The positive dashed line indicates years with values exceeding 0.5, corresponding to extreme El Niño and TNA events.

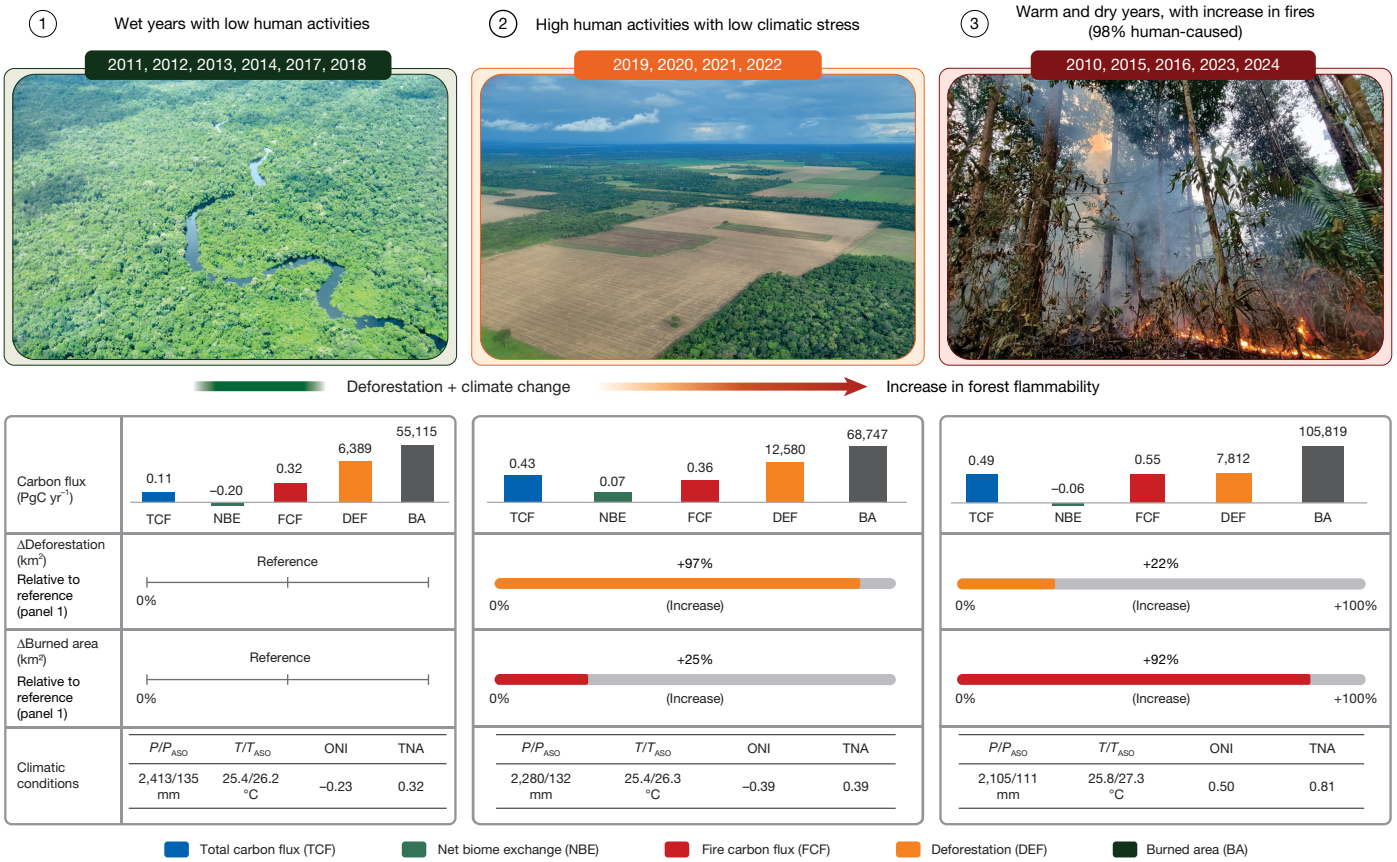


Fig. 5 | Schematic grouping summary. Schematic summary of the main results of the 15-year groups: (1) wet years, with low human activity of deforestation and burning area (0.11 ± 0.08 PgC yr^{-1}); (2) low climatic stress years, with high human activity, mainly by deforestation (0.43 ± 0.13 PgC yr^{-1}); and (3) warm and dry years, with high fire increase, 98% caused by humans (0.49 ± 0.07 PgC yr^{-1}). *P*, annual accumulated precipitation; P_{ASO}, monthly mean precipitation for August, September and October; *T*, annual mean temperature; T_{ASO}, monthly mean temperature for August, September and October.

and burned area, which were, respectively, 38% and 52% higher than in group 1. The annual mean temperature was similar to that of group 1, starting colder than normal and warming progressively as strong TNA and El Niño events became unprecedented drought and heat wave[34,35] (Fig. 4).

While 2023 began after 3 years of La Niña, 2024 began in the middle of strong El Niño and TNA events, which made its outcome completely different. The year 2024 exhibited the highest carbon emissions (0.81 ± 0.09 PgC yr^{-1}) in the 15-year record (Extended Data Tables 2 and 3 and Extended Data Fig. 7), 605% higher than that of group 1. It was also the hottest, driest and most strongly degraded by fire over the past two decades[36]. Annual temperatures were 1.2 °C higher than in group 1, and annual precipitation was 462 mm lower than in group 1. The burned area was 182% higher than in group 1, producing the most extensive burned area observed since 2010 in Amazonia (Fig. 3a and Extended Data Tables 2 and 3). Following the reinstatement of public policies to curb deforestation in 2023 (ref. 13), fire became a widespread tool for deforestation. In 2024, PRODES identified that 38% deforestation was caused by fire[37]. Most Amazonian wildfires are intentionally set, and severe droughts exacerbate their extent and intensity[15,29,31,37].

More detailed subregional (RBA, ALF, SAN, TTC) analyses are provided in Extended Data Tables 2 and 3, Extended Data Figs. 2 and 3, Supplementary Discussion 3 and Supplementary Figs. 3–5.

Conclusion

The 15-year annual mean Amazonia carbon balance was 0.32 ± 0.08 PgC yr^{-1} (FCF, 0.40 ± 0.07 PgC yr^{-1}; NBE, −0.08 ± 0.12 PgC yr^{-1}). The pronounced interannual variability (−0.12 PgC yr^{-1} to 0.75 PgC yr^{-1}) underscores the need for decadal-scale analyses to accurately define the role of Amazonia in the global carbon cycle, and it is also important to consider spatial representativeness, given the large variability across the subregions studied. Long-term deforestation and degradation have reduced annual precipitation by about 8% over the past 46 years and dry-season peak precipitation by about 20%, while increasing annual mean temperature by 1.13 ± 0.13 °C and dry-season temperature by 1.81 ± 0.18 °C. The grouping of years, in three distinct scenarios (Fig. 5), showed what Amazonia represents for the global carbon balance in each of these scenarios: (1) wet years, with low human activities (0.11 ± 0.08 PgC yr^{-1}); (2) low climatic stress years with high human activities (0.43 ± 0.13 PgC yr^{-1}); and (3) warm and dry years, associated with intense increase of fires, essentially human-caused (0.49 ± 0.07 PgC yr^{-1}). It is important to note that groups 2 and 3 do not differ significantly in carbon emissions, and both are dominated by deforestation and biomass burning, respectively. It is also noteworthy that the NBE across all three groups is close to neutral, indicating that direct human activities are the main risks to the Amazon. Drastic fire reduction is therefore essential to avert a tipping point, especially as escalating climate stress amplifies human impacts, and vice versa. Based on the consequences of the very strong El Niño 2015–2016 in the southeast Amazon region, which has become an increasing source of carbon, similar consequences are expected after the strong El Niño and TNA events in 2023–2024 for Amazonia. These results highlight the urgent need to implement a zero-deforestation policy, strengthen controls on biomass burning and prioritize forest restoration programmes.

Online content

Any methods, additional references, Nature Portfolio reporting summaries, source data, extended data, supplementary information, acknowledgements, peer review information; details of author contributions and competing interests; and statements of data and code availability are available at https://doi.org/10.1038/s41586-026-11168-1.

1. Gatti, L. V. et al. Amazonia as a carbon source linked to deforestation and climate change. *Nature* **595**, 388–393 (2021).
2. Leite-Filho, A. T., Costa, M. H. & Fu, R. The southern Amazon rainy season: the role of deforestation and its interactions with large-scale mechanisms. *Int. J. Climatol.* **40**, 2328–2341 (2020).
3. Leite-Filho, A. T., Soares-Filho, B. S., Davis, J. L., Abrahão, G. M. & Börner, J. Deforestation reduces rainfall and agricultural revenues in the Brazilian Amazon. *Nat. Commun.* **12**, 2591 (2021).
4. Fu, R. et al. Increased dry-season length over southern Amazonia in recent decades and its implication for future climate projection. *Proc. Natl Acad. Sci. USA* **110**, 18110–18115 (2013).
5. Franco, M. A. et al. How climate change and deforestation interact in the transformation of the Amazon rainforest. *Nat. Commun.* **16**, 7944 (2025).
6. Brienen, R. J. W. et al. Long-term decline of the Amazon carbon sink. *Nature* **519**, 344–348 (2015).
7. Phillips, O. L. & Brienen, R. J. W. Carbon uptake by mature Amazon forests has mitigated Amazon nations' carbon emissions. *Carbon Balance Manage.* **12**, 1 (2017).
8. Hubau, W. et al. Asynchronous carbon sink saturation in African and Amazonian tropical forests. *Nature* **579**, 80–87 (2020).
9. Feron, S. et al. South America is becoming warmer, drier, and more flammable. *Commun. Earth Environ.* **5**, 501 (2024).
10. Staal, A. et al. Hysteresis of tropical forests in the 21st century. *Nat. Commun.* **11**, 4978 (2020).
11. Longo, M. et al. Degradation and deforestation increase the sensitivity of the Amazon Forest to climate extremes. *Environ. Res. Lett.* **20**, 054024 (2025).
12. Doughty, C. E. et al. Tropical forests are approaching critical temperature thresholds. *Nature* **621**, 105–111 (2023).
13. Gatti, L. V. et al. Increased Amazon carbon emissions mainly from decline in law enforcement. *Nature* **621**, 318–323 (2023).
14. Marengo, J. A. Long-term variability, extremes and changes in temperature and hydrometeorology in the Amazon region: a review. *Acta Amaz.* **54**, e54es22098 (2024).
15. Aragão, L. E. O. C. et al. 21st Century drought-related fires counteract the decline of Amazon deforestation carbon emissions. *Nat. Commun.* **9**, 536 (2018).
16. Costa, M. H. et al. The physical hydroclimate system of the Amazon. In *Amazon Assessment Report 2021* (eds Nobre, C. et al.) Ch. 5 https://doi.org/10.55161/HTSD9250 (UN Sustainable Development Solutions Network, 2021).
17. Costa, M. H. et al. Biogeophysical cycles: water recycling, climate regulation. In *Amazon Assessment Report 2021* (eds Nobre, C. et al.) Ch. 7 https://doi.org/10.55161/KKHX1998 (UN Sustainable Development Solutions Network, 2021).
18. Esquivel-Muelbert, A. et al. Tree mode of death and mortality risk factors across Amazon forests. *Nat. Commun.* **11**, 5515 (2020).
19. Malhi, Y. et al. Biogeochemical cycles in the Amazon. In *Amazon Assessment Report 2021* (eds Nobre, C. et al.) Ch 6 https://doi.org/10.55161/TAKR3454 (UN Sustainable Development Solutions Network, 2021).
20. Malhi, Y. et al. Comprehensive assessment of carbon productivity, allocation and storage in three Amazonian forests. *Glob. Chang. Biol.* **15**, 1255–1274 (2009).
21. PRODES. Amazon Deforestation Monitoring Project (PRODES/INPE) https://terrabrasilis.dpi.inpe.br/app/map/deforestation (2025).
22. MMA GOV BR. PPCDAm http://redd.mma.gov.br/pt/acompanhamento-e-a-analise-de-impacto-das-politicas-publicas/ppcdam (2017).
23. West, T. A. P. & Fearnside, P. M. Brazil's conservation reform and the reduction of deforestation in Amazonia. *Land Use Policy* **100**, 105072 (2021).
24. Mapbiomas_Amazonia. The MapBiomas Amazon Collection 10 includes annual land use and land cover data for the period 1985-2024 https://plataforma.brasil.mapbiomas.org/ (2025).
25. MapBiomas. MapBiomas Fogo. *Annual and Cumulative Burned Area and Coverage (Collection 4*) https://brasil.mapbiomas.org/en/mapbiomas-fogo (2025).
26. ONI. Oceanic Nino Index, Climate Prediction Center, NOAA https://www.cpc.ncep.noaa.gov/products/analysis_monitoring/ensostuff/detrend.nino34.ascii.txt (2025).
27. ERA5. European Centre for Medium-Range Weather Forecasts, (ECMWF) - Copernicus Climate Data Store (CDS) https://cds.climate.copernicus.eu/datasets (2025).
28. Climate Prediction Center. Official NOAA CPC ENSO Strength Probabilities. *NOAA Climate Prediction Center* https://cpc.ncep.noaa.gov/products/analysis_monitoring/enso/roni/strengths/ (2026).
29. Brando, P. M. et al. Tipping points of Amazonian forests: beyond myths and toward solutions. *Annu. Rev. Environ. Resour.* **50**, 97–131 (2025).
30. Flores, B. M. et al. Critical transitions in the Amazon forest system. *Nature* **626**, 555–564 (2024).
31. Alencar, A. A., Brando, P. M., Asner, G. P. & Putz, F. E. Landscape fragmentation, severe drought, and the new Amazon forest fire regime. *Ecol. Appl.* **25**, 1493–1505 (2015).
32. Anderson, L. O. et al. Vulnerability of Amazonian forests to repeated droughts. *Philos. Trans. R. Soc. B Biol. Sci.* **373**, 20170411 (2018).
33. Alencar, A. A. C. et al. Long-term Landsat-based monthly burned area dataset for the Brazilian biomes using deep learning. *Remote Sens.* **14**, 2510 (2022).
34. Santos Fleischmann, A. et al. Extreme warming of Amazon waters in a changing climate. *Science* **390**, 606–611 (2025).
35. Espinoza, J.-C. et al. The new record of drought and warmth in the Amazon in 2023 related to regional and global climatic features. *Sci. Rep.* **14**, 8107 (2024).
36. Bourgoin, C. et al. Extensive fire-driven degradation in 2024 marks worst Amazon forest disturbance in over 2 decades. *Biogeosciences* **22**, 5247–5256 (2025).
37. Messias, C. G. et al. Unaccounted for nonforest vegetation loss in the Brazilian Amazon. *Commun. Earth Environ.* **5**, 451 (2024).

Publisher's note Springer Nature remains neutral with regard to jurisdictional claims in published maps and institutional affiliations.

Open Access This article is licensed under a Creative Commons Attribution 4.0 International License, which permits use, sharing, adaptation, distribution and reproduction in any medium or format, as long as you give appropriate credit to the original author(s) and the source, provide a link to the Creative Commons licence, and indicate if changes were made. The images or other third party material in this article are included in the article's Creative Commons licence, unless indicated otherwise in a credit line to the material. If material is not included in the article's Creative Commons licence and your intended use is not permitted by statutory regulation or exceeds the permitted use, you will need to obtain permission directly from the copyright holder. To view a copy of this licence, visit http://creativecommons.org/licenses/by/4.0/.

© The Author(s) 2026

Methods

Sites, air sampling and analysis

Here, we report CO_2 and CO measurement results from the four Amazonian aircraft vertical profile sites of the CARBAM project[38] (SAN: 2.86° S 54.95° W; ALF: 8.80° S 56.75° W; RBA: 9.38° S 67.62° W; in 2010–2012 for TAB: 5.96° S 70.06° W; and since 2013 for TEF: 3.39° S 65.60° W, and since 2022 for CZS: 7.00° S 72.50° W), detailed in refs. 1,13. The regions of influence for the four sites representing the northeast (SAN), southeast (ALF), southwest (RBA) and northwest Amazon region (TAB, 2010–2012; TEF, 2013–2021; CZS, 2022–2024) are shown in Extended Data Fig. 2c–h. Our samples were typically collected twice per month, totalling 1,017 vertical profiles over 15 years, in a descending spiral from 4,420 m to about 300 m a.s.l. In 2015, the vertical profile sampling was stopped in April at all sites and resumed in November at RBA. In 2016, vertical profiles were performed only at RBA and ALF. The vertical profiles were usually taken between 12:00 and 13:00 local time. Air samples were analysed by a non-dispersive infrared analyser for CO_2 and by gas chromatography with HgO reduction detection for CO. The detailed analytical and sampling methods were presented in previous studies[1,13].

Amazonia carbon study area

We defined the Amazonia study area according to subregions from ref. 39 and biomes from ref. 40, in which the studied area in Amazonia was determined to include only the forest ecosystems subregions: Amazonia stricto sensu, Guianas and Gurupi, with a total area of 6,700,798 km^2.

Annual mean vertical profiles

The annual mean VP for each site was calculated by first producing the monthly mean for each height and then the annual mean for each height. The annual mean ΔVP for each site and for Amazonia was calculated by subtracting the corresponding background (BKG) for each VP and each height (Fig. 2 and Extended Data Fig. 3). To calculate the Amazonia annual mean VP, we applied the same method used to obtain the Amazonia annual mean flux and balance. To scale to the whole of Amazonia, we divided it into three regions (see ref. 13 and Supplementary Fig. 5). To compose the VP for region 1 (SAN + ALF), we calculated the weighted mean CO_2 concentration at each height, proportional to the area of each region. To calculate the VP for region 2 (RBA + TAB, 2010–2012; RBA + TEF, 2013–2021; RBA + CZS, 2022–2024), the same procedure was used as in region 1. And for VP of region 3, the remaining Amazonia area not covered by the regions of influence of the vertical profile, we used the same VP as region 2. To compose the VP for Amazonia, the weighted mean for each height CO_2 concentration was calculated, considering the three regions for each height (Supplementary Fig. 5).

Estimation of carbon fluxes

We used a column budget technique to estimate TCF, FCF and NBE, which consists of the difference between CO_2 mole fraction measured in the vertical profile and the estimated background mole fraction[41] (ΔCO_2), considering the travel time of air parcels along the trajectory from the coast to the site (equation (1)), following the methodology in refs. 1,13,42.

$$F_x = \int_{z=0(\mathrm{agl})}^{4.4\ \mathrm{km(asl)}} \frac{\Delta X}{t(z)} \mathrm{d}z. \quad (1)$$

Background

Background mole fractions were estimated according to the methodology described in ref. 41, using the geographical position of each air-mass back-trajectory from the HYSPLIT model[43] when it intersects two virtual limits: (1) a latitude limit, from the Equator southwards at 30° W and (2) a line between two observation sites at Ragged Point, Barbados (RPB), and Ascension Island, the United Kingdom (ASC), from NOAA/GML. We used CO_2 (ref. 44) and CO (ref. 45) concentrations from the NOAA/GML Carbon Cycle Cooperative Global Air Sampling Network to determine the background.

Carbon fire fluxes

We calculated fire emissions according to the methods published in refs. 1,13. We used observed CO/CO_2 ratios by site from 2010 to 2024 (CO/CO_2, ppb CO per ppm CO_2) from measured CO mole fractions. The CO/CO_2 ratios were calculated from clearly identifiable plumes in the vertical profiles during the dry season along period study (39 VP ALF $CO/CO_2 = 60.7 \pm 30.7$ ppb ppm^{-1}; 35 VP SAN $CO/CO_2 = 56.1 \pm 20.4$ ppb ppm^{-1}; 44 VP RBA $CO/CO_2 = 67.7 \pm 24.1$ ppb ppm^{-1}; and 19 VP TTC (TAB_TEF_CZS) $CO/CO_2 = 74.2 \pm 29.1$ ppb ppm^{-1}), which represents how many ppb CO is emitted for each 1 ppm CO_2 during burning process. To calculate CO_2 from fire, we used the CO flux and subtracted it from natural CO emissions (equation (2)). After the step $F_{CO} - F_{CO}^{Natural}$, we used the CO/CO_2 ratio to estimate the amount of CO_2 from fire. NBE represents all processes from natural sources and sinks and all anthropogenic non-fire emissions (or after fire, without CO emissions) (NBE = total − fire).

$$\mathrm{FC_{Fire}} = R_{CO_2:CO}(F_{CO} - F_{CO}^{Natural}). \quad (2)$$

Flux uncertainty analysis by Monte Carlo error propagation

Flux uncertainties were estimated using Monte Carlo error propagation (1,000 iterations). CO_2 measurement uncertainty was 0.03 ppm, and background (BKG) uncertainties were derived from residuals to the fitted CO_2 smooth curve, according to ref. 1. Uncertainties in back-trajectory travel times[13] were also included. For carbon fire emissions and NBE, uncertainties in CO/CO_2 ratios, CO fluxes and a 25% uncertainty in natural CO emissions were considered. VP flux uncertainties were derived from the Monte Carlo ensemble. Monthly uncertainties were estimated using pooled standard deviation to account for intra-month variability within the annual mean flux, and period uncertainties were calculated using the quadratic mean.

An additional source of uncertainty is the limitation on sampling to 4.4 km a.s.l. Transit times of air parcels from the coast to sampling sites, based on HYSPLIT, can vary, with mean trajectory times of 2.6 days for SAN, 5.3 days for ALF, 6.6 days for RBA, 5.7 days for TAB, 5.0 days for TEF and 7.6 days for CZS. The convective process, together with long travel times of air masses, can represent loss of carbon sources and sink contributions from the surface, because our vertical profiles start at 4.4 km. Comparing the background concentration and the top of vertical profiles is one way to verify potential information loss[1,13]. According to the method we use, the flux is obtained by subtracting the measured CO_2 mole fraction in the VP from the background concentration, accounting for the integration time (equation (1)). During the dry season, the loss of information is larger to positive (VP > BKG), because during the burning season (peak of the dry season), the top of VP starts with a higher CO_2 concentration than BKG due to convective processes driven by biomass burning.

A previous study[46] proposed a correction of our gas concentration measurements based on a comparison of laboratory analyses of samples collected on 12 vertical profiling flights above Manaus in 2017–2019. The in situ measurements were made with a cavity ring-down spectrometer (CRDS), and discrete flask samples (PFPs) collected on the same flights were analysed in the laboratory. Some of the continuous CRDS measurements differed from those determined in the laboratory from flask samples (PFP) collected on the same flights (Figure A4 in ref. 46). Based on linear regression of $N = 158$ paired CRDS-PFP measurements, ref. 46 reported that water vapour content explained only 13% of the variance in the CRDS-PFP differences (Figure A7 in ref. 46). Nevertheless, ref. 46 proposed applying this regression relationship to adjust all laboratory measurements. Applying such an adjustment would conflate

multiple methodological differences between the two sampling and analytical systems. The regression in ref. 46 compares independent instruments sampling distinct air parcels under different pressures, flow rates and materials. The proposed correction assumes that the in situ CRDS measurements are accurate, that the laboratory analyses are biased, that discrepancies arise solely from water vapour, and that the regression relationship can be extrapolated to approximately 13,319 laboratory measurements collected over 15 years. For these reasons, the proposed adjustment was not applied in this study. LaGEE measurements used in this study are internally consistent across the full temporal and spatial domain.

An additional source of uncertainty is addressed in the calculation of fire carbon emissions and NBE. Over time, the forest is becoming drier and hotter. These changes promote a lower CO/CO_2 ratio. The use of a single mean CO/CO_2 ratio is another source of uncertainty, leading to lower fire emissions than those observed in recent years because the ratio tends to decline over time. It is likely that carbon emissions from fires were higher than our averages for 2023 and 2024 indicate, because both were drought years.

Missing data imputation

We used the missForest algorithm to impute missing monthly TCF and FCF data at the ALF, SAN, RBA and TAB_TEF_CZS (TTC) sites. These gaps resulted from sampling and logistical issues in the laboratory. The missForest method is a non-parametric imputation approach based on random forests[47,48], and we implemented it in R language[49] through the missForest package[50]. To estimate missing values for TCF and FCF[1,13], we included the following monthly variables in the imputation process: temperature (T), precipitation (P), vapour pressure deficit (VPD), ONI, TNA index, EVI, burned area (BA) and fire spots (FS). The missing data gaps were imputed using average values calculated from 1,000 runs of missForest. The normalized root mean square errors obtained for FC_{Total} and FC_{Fire} were 0.0014 and 0.0012 for ALF, 0.0011 and 0.0010 for RBA, 0.0055 and 0.0053 for SAN and 0.0018 and 0.0016 for TTC, respectively. NBE missing data were calculated by subtracting the fire from TCF.

Regions of influence

We define regions of influence as those areas covered by the density of back-trajectories[51]. We updated the calculations for the regions of influence used in our published CO_2 papers[1]. In this study, the regions received two treatment steps. In the first step, we calculated back trajectories for altitudes lower than 1,300 m. As we have only four heights below 1,300 m, the density of trajectories could be reduced, compromising the representativeness. To better characterize atmospheric circulation over the quarters and years, we calculated trajectories at each sampling height (>1,300 m) twice a week, at the same locations and time of day, over the 15 years for each VP sampling site. A second treatment in the grid cells was done to increase the weight for the grid cells near the sample site. We normalized the weight for the region of influence to be from 0 to 1. First, the grid with a value of 1 was calculated by disregarding 2.5% of the grids with the highest values, thereby increasing the area of the grid region with a value of 1. It was considered a regular grid of 1° × 1° generated in the WGS 84 georeference system (EPSG:4326).

Precipitation, temperature, VPD and EVI data

We used the quarterly regions of influence maps as spatial weighting functions for all studied parameters to determine how each parameter influenced the carbon flux and for the missing data imputation process (missForest), following ref. 4. We used the GPCP database (http://eagle1.umd.edu/GPCP_ICDR/GPCP_Monthly.html), v.1.3, for precipitation analysis (described in refs. 52–54), which contains daily data at a 1° × 1° latitude–longitude resolution. We used 2-m temperatures from ERA-5 that are monthly means of daily means since 1959, and which were used with a resolution of 0.25° × 0.25° latitude–longitude, obtained from the European Centre for Medium-Range Weather Forecasts (ECMWF)[27,55]. The VPD product is a measure of the indirect vapour pressure deficit in kPa (resolution of 2.5 arcmin) of monthly means of temperature and humidity, provided by the Climatic Research Unit Ts4.0 (ref. 56). The dataset was resampled to a 1° × 1° spatial resolution using the monthly mean. The EVI is a vegetation index that aims to estimate the fraction of photosynthetically active radiation (fPAR) from terrestrial vegetation. The EVI product used[57] was the MANVI: Moderate Resolution Imaging Spectroradiometer (MODIS) multiangle implementation of atmospheric correction nadir-solar (see the methods in ref. 13).

Burned area

Two products of burned area (BA) were used: (1) for all annual burned areas, the BA from MapBiomas was used, integrating all types of vegetation that were burned (primary and secondary forest, pasture, agriculture and others), from the MapBiomas Fire Collection 4 (ref. 25; https://brasil.mapbiomas.org). MapBiomas Fire was validated with a global accuracy of 89% (ref. 33); (2) for monthly BA (used only for missForest calculation), MODIS products were used: MODIS Collection 6 MCD64A1 burned area product[13,58].

Deforestation

The procedures to retrieve deforestation as geographic data built by PRODES/INPE[21] based on a historical series of Landsat images provide deforestation annual increments in the Brazilian Amazon. Detailed information on the PRODES methodology is available and can be accessed at http://urlib.net/rep/8JMKD3MGP3W34R/443H3RE (ref. 59). The dataset accuracy is 93.5 (ref. 60). We used the data period from 2010 to 2024. Using QGIS software, a 0.25° × 0.25° grid was generated for the entire Brazilian Amazon, which was filled with the absolute values of deforested area calculated for each cell and each year of the series. The mean deforestation area was calculated for the period 2010–2024 within each grid cell. Annual deforestation data correspond to the deforested area mapped by the PRODES project in a given year for Amazon forests.

Monthly deforestation and degradation

Monthly deforestation and degradation data correspond to either the deforestation alerts (clear cut, deforestation with vegetation, and mining) or degradation alerts (ordered selective logging, disordered selective logging, burns and degradation) captured by the DETER[61] Amazon system in a given month. This dataset is produced daily by the visual interpretation of medium spatial resolution optical imagery of National Institute for Space Research (INPE) and, although not a full estimate of deforestation and degradation in the Amazon, can indicate variations in deforestation patterns over time[33,62]. We used the raw version of the dataset provided by INPE that included both password-protected data and data collected from August 2015.

Fire spots

Fire spots in Pan-Amazonia between 2010 and 2024 and burned area in Brazilian Amazon were retrieved from the BDQueimadas wildfire monitoring program of INPE[63] (see the methods in ref. 13).

ONI

Warm (El Niño) and cold (La Niña) periods based on a threshold of ±0.5 °C for the ONI, 3-month running mean of ERSST v.5 SST anomalies in the Niño 3.4 region (5° N–5° S, 120° W–170° W), based on centred 30-year base periods updated every 5 years (ref. 26). To analyse the intensity of the events, we used the ONI classification anomaly[28]—for El Niño events, weak (0.5–0.9 °C), moderate (1.0–1.4 °C), strong (1.5–1.9 °C), and very strong (≥2.0 °C).

TNA index

The TNA index was computed as the mean sea-surface temperature (SST) anomaly over the region 23.5° N–5.5° N and 57.5° W–15° W (ref. 64).

Monthly SST fields were obtained from ERA5 (0.25°), and anomalies were derived relative to a 30-year climatological baseline (1971–2000), consistent with standard TNA calculations[27]. We used the same ONI anomaly classification to analyse the intensity of the TNA warming events.

Statistical analysis

Annual data (2010–2024) for the Amazon included TCF, precipitation (P), temperature (T), ONI, TNA index, fire spots (FS), burned area (BA), annual deforestation (DEF) and accumulated deforestation (DEF_acc). Variable distributions and homogeneity of variance were assessed using the Shapiro–Wilk and Levene's tests (Supplementary Table 1), respectively. Although most variables met normality assumptions, robust statistical approaches were adopted because of the small sample size ($n = 15$) and potential deviations from Gaussian behaviour typical of environmental datasets (Supplementary Discussion 3). Principal component analysis was applied to standardized data, with the first two components considered to represent the dominant variability. The k-means clustering ($k = 3$) was performed in the principal component analysis space, with cluster characteristics summarized in a standardized heatmap. The optimal number of clusters was determined using the average silhouette width (Extended Data Fig. 4).

Group differences among clusters were assessed using Welch's analysis of variance (Supplementary Table 1), which is robust to heteroscedasticity and unequal sample sizes. When significant differences were detected ($P < 0.05$), pairwise comparisons were conducted using the Games–Howell post hoc test (Supplementary Table 1), which does not assume equal variances and appropriately controls the type I error rate under these conditions. This approach provides a consistent and reliable framework for identifying differences among clusters in environmental variables (Supplementary Discussion 2). All analyses were conducted in R language[49].

Amazonia pasture, soybean and mining area

We obtained annual estimates of pasture, soybean cropland and mining area across Amazonia from the MapBiomas Collection 10[24] dataset (30 m spatial resolution). Annual land-cover maps were used to isolate class-specific pixels (pasture, soybean and mining) and to compute their corresponding areas (km^2) within the Amazonia carbon study area. This approach provided a consistent time series of land-use expansion and persistence for 2000–2024.

Lightning-associated wildfires

After 2017, in group 3, the years with accurate data were 2023 and 2024, when a more accurate cloud-to-ground lightning dataset was available. We used cloud-to-ground strokes from the Earth Networks Total Lightning Network (ENTLN)[65]. In South America, particularly in Amazonia, ENTLN lacks a dense sensor network comparable to that in other regions of Brazil. Even so, it operates with a stroke detection efficiency above 50% (corresponding to a flash detection efficiency above 80%) and a mean location accuracy below 1 km. Just for reference, in regions with high sensor densities, after the 2021 upgrade, the ENTLN reaches cloud-to-ground flash detection efficiency levels above 95% and median location accuracy below 100 m (ref. 66). Although performance depends on regional sensor coverage, ENTLN is considered one of the most advanced and reliable lightning networks globally[67]. Active fires used in this study were provided by the Visible Infrared Imaging Radiometer Suite on the Suomi National Polar-Orbiting Partnership satellite, with a spatial resolution of 375 m. The Visible Infrared Imaging Radiometer Suite 375 m active fire product provides geolocation accuracy of the order of one pixel (about 375 m), with typical sub-pixel geolocation uncertainties (about 70 m), ensuring reliable spatial representation of fire locations. All overpasses, day and night, were used from the Wildfire Monitoring Program of the INPE, available at http://www.inpe.br/queimadas/ (ref. 63). To assess lightning-associated wildfire among all cloud-to-ground lightning strokes, we identified probable lightning candidates that occurred up to 72 h (3 days) before active fire detection, using a fixed buffer radius of 1 km around each active fire and accounting for the location accuracy of both datasets. A detailed description of lightning candidate characteristics in Brazil is provided in ref. 68.

Data availability

The CO_2 and CO data, the calculated BKG CO_2 and CO, and the time trajectory for each flask/height/day that were used to calculate the sites (TAB_TEF_CZS, SAN, ALF and RBA) and Amazon fluxes and balance that supported the findings of this study are available in the PANGAEA Data Archive, for data from 2010 to 2024 (https://doi.org/10.1594/PANGAEA.988417)[38].

38. Gatti, L. V. et al. CO_2 vertical profiles on four sites over Amazon from 2010 to 2024. *PANGAEA* https://doi.org/10.1594/PANGAEA.988417 (2026).
39. Eva, H., Huber, O. (eds). *A Proposal for Defining the Geographical Boundaries of Amazonia*. JRC68635 (Office for Official Publications of the European Communities, 2005).
40. Olson, D. M. et al. Terrestrial ecoregions of the world: a new map of life on Earth: a new global map of terrestrial ecoregions provides an innovative tool for conserving biodiversity. *BioScience* **51**, 933–938 https://doi.org/10.1641/0006-3568(2001)051[0933:TEOTWA]2.0.CO;2 (2001).
41. Domingues, L. G. et al. A new background method for greenhouse gases flux calculation based in back-trajectories over the Amazon. *Atmosphere* **11**, 734 (2020).
42. Miller, J. B. et al. Airborne measurements indicate large methane emissions from the eastern Amazon basin. *Geophys. Res. Lett.* **34**, L10809 (2007).
43. Stein, A. F. et al. NOAA's HYSPLIT atmospheric transport and dispersion modeling system. *Bull. Am. Meteorol. Soc.* **96**, 2059–2077 (2015).
44. Lan, X. et al. *Atmospheric Carbon Dioxide Dry Air Mole Fractions from the NOAA GML Global Greenhouse Gas Reference Network, Carbon Cycle Cooperative Global Air Sampling Network: 1967 - Present, Version: 2025-08-15* https://doi.org/10.15138/wkgj-f215 (2025).
45. Petron, G. et al. *Atmospheric Carbon Monoxide Dry Air Mole Fractions from the NOAA GML Carbon Cycle Cooperative Global Air Sampling Network, 1988-2024, Version: 2025-08-11* https://doi.org/10.15138/33bv-s284 (2025).
46. Botia, S. et al. Combined CO2 measurement record indicates Amazon forest carbon uptake is offset by savanna carbon release. *Atmos. Chem. Phys.* **25**, 6219–6255 (2025).
47. Jiang, N. & Riley, M. L. Exploring the utility of the random forest method for forecasting ozone pollution in SYDNEY. *J. Environ. Prot. Sustain. Dev.* **1**, 245–254 (2015).
48. Stekhoven, D. J. & Buhlmann, P. missForest–non-parametric missing value imputation for mixed-type data. *Bioinformatics* **28**, 112–118 (2012).
49. R Core Team. *R: A Language and Environment for Statistical Computing* https://www.r-project.org (R Foundation for Statistical Computing, 2024).
50. Stekhoven, D. J. missForest: Nonparametric missing value imputation using Random Forest. R version 1.4. https://doi.org/10.32614/CRAN.package.missForest (2013).
51. Cassol, H. L. G. et al. Determination of region of influence obtained by aircraft vertical profiles using the density of trajectories from the HYSPLIT model. *Atmosphere* **11**, 1073 (2020).
52. Adler, R. F. et al. The global precipitation climatology project (GPCP) monthly analysis (new version 2.3) and a review of 2017 global precipitation. *Atmosphere* **9**, 138 (2018).
53. Huffman, G. J. et al. Global precipitation at one-degree daily resolution from multisatellite observations. *J. Hydrometeorol.* **2**, 36–50 (2001).
54. Physical Sciences Laboratory. *Global Precipitation Climatology Project (GPCP) Monthly Analysis Product* https://psl.noaa.gov/data/gridded/data.gpcp.html (2025).
55. Hersbach, H. et al. The ERA5 global reanalysis. *Q. J. R. Meteorol. Soc.* **146**, 1999–2049 (2020).
56. Abatzoglou, J. T., Dobrowski, S. Z., Parks, S. A. & Hegewisch, K. C. TerraClimate, a high-resolution global dataset of monthly climate and climatic water balance from 1958–2015. *Sci. Data* **5**, 170191 (2018).
57. Dalagnol, R., Wagner, F. H., Galvão, L. S., Oliveira, L. E. & Aragao, L. E. O. e. C. The MANVI product: MODIS (MAIAC) nadir-solar adjusted vegetation indices (EVI and NDVI) for South America. *Zenodo* https://doi.org/10.5281/zenodo.3159487 (2019).
58. Giglio, L., Boschetti, L., Roy, D. P., Humber, M. L. & Justice, C. O. The Collection 6 MODIS burned area mapping algorithm and product. *Remote Sens. Environ.* **217**, 72–85 (2018).
59. de Almeida, C. A. et al. *Methodology for Forest Monitoring Used in PRODES and DETER Projects*. INPE, version: 2021-01-26 http://urlib.net/rep/8JMKD3MGP3W34R/443H3RE (INPE, 2021).
60. Maurano, L. E. P., Escada, M. I. S. & Renno, C. D. Padrões espaciais de desmatamento e a estimativa da exatidão dos mapas do PRODES para Amazônia Legal Brasileira. *Ciênc. Florest.* **29**, 1763–1775 (2019).
61. DETER. *Real-Time Deforestation Detection System, Terrabrasilis, INPE* https://terrabrasilis.dpi.inpe.br/app/dashboard/alerts/biomes/amazonia-nb/aggregated/# (INPE, 2025).
62. Alencar, A. et al. *MapBiomas Degradation Module BETA - Algorithm Theoretical Basis Document (ATBD)* https://doi.org/10.58053/MapBiomas/XPA9ZB (MapBiomas, 2024).
63. *BDQueimadas. INPE Biomass burning Program* https://terrabrasilis.dpi.inpe.br/queimadas/bdqueimadas (2025).
64. Enfield, D. B., Mestas-Nuñez, A. M., Mayer, D. A. & Cid-Serrano, L. How ubiquitous is the dipole relationship in tropical Atlantic sea surface temperatures? *J. Geophys. Res. Oceans* **104**, 7841–7848 (1999).
65. DiGangi, E., Lapierre, J., Stock, M., Hoekzema, M. & Cunha, B. Analyzing lightning characteristics in central and southern South America. *Electr. Power Syst. Res.* **213**, 108704 (2022).

66. Zhu, Y., Stock, M. & Lapierre, J. Upgrades of the Earth Networks Total Lightning Network in 2021. *Remote Sens.* **14**, 2209 (2022).
67. Virts, K. S., Lang, T. J., Buechler, D. E. & Bitzer, P. M. Bayesian analysis of the detection performance of the lightning imaging sensors. *J. Atmos. Ocean. Technol.* **41**, 441–455 (2024).
68. Schumacher, V. et al. Characteristics of lightning-caused wildfires in central Brazil in relation to cloud-ground and dry lightning. *Agric. For. Meteorol.* **312**, 108723 (2022).

Acknowledgements We thank O. Tarasova (WMO) for the QCF grant. We thank numerous people at NOAA/GML who provided advice and technical support for air sampling and measurements in Brazil, and the pilots and technical teams at aircraft sites who collected the air samples. We thank J. F. Mueller for providing modelled biogenic CO fluxes. We thank Tasso Azevedo, Ana Inoue and the Instituto Imbuzeiro.

Author contributions L.V.G. and J.B.M. conceived of the basin-wide measurement programme and approach; L.V.G., C.L.C., J.C.G.B., A.S.D. and J.B.M. wrote the paper; C.N., J.A.B., E.C. and J.E.J. contributed with ideas, commented and reviewed the manuscript; L.V.G. and C.L.C. performed the results analysis; L.G.D., A.H.S., L.M. and L.V.G. contributed with region of influence study; M.S.R., E.A., C.L.C., L.M., J.C.G.B. and L.V.G. contributed with climate-data-weighted studies; J.M. contributed with climate analysis; M.S.R., C.G.M., V.L.C., L.S. and C.A. contributed with deforestation and degradation analysis; L.G.D., C.S.C.C., L.M., R.A.L.N., F.M.d.S., G.B.M.M., F.L.L. and C.S. contributed with CO_2 and CO concentration analysis; J.C.G.B. and M.M. contributed with maps and processing data analysis; L.V.G. contributed with biogenic CO estimation; C.L.C. produced the missForest; C.L.C., V.L.C. and S.M.C. produced statistical analysis; J.C.G.B. produced data on human economic activities in the Amazon region; D.E.C. and A.A.C.A. provided burned area quantification; X.L. and G.P. provided RPB, ASC and CPT CO_2 and CO data, respectively; V.S. and K.P.N. contributed with fire and lightning study.

Funding The scientific research projects that funded the GHG measurement program with vertical profiles in Amazonia, since 2009 are as follows: (1) the State of São Paulo Science Foundation (FAPESP): 16/02018-2—partially financed the measurements, laboratory costs and scholarship for the period 2018–2023; 11/51841-0—partially financed the measurements, laboratory costs and scholarship, 2013–2015; 08/58120-3—partially financed the measurements, laboratory costs and scholarship, 2010–2013; 21/09020-0—postdoc scholarship related to the CO_2 and CO statistical analysis, 2021–2023; (2) the UK Environmental Research Council (NERC) AMAZONICA project (NE/F005806/1), partially financing measurements, laboratory costs, and a scholarship for the period 2009–2014; (3) the NASA grants: 11-CMS11-0025, partially financed the measurements, laboratory costs and scholarship for the period 2012–2013; NRMJ1000-17-00431, partially financed the measurements, laboratory costs and scholarship for the period 2016–2017; (4) 7FP EU (283080), GEOCARBON project, partially financed the measurements, laboratory costs and scholarship for the period 2012–2015; (5) the ERC/Horizon 2020 (649087), ASICA project, partially financed the measurements, laboratory costs and scholarship for the period 2017–2020; (6) CNPq: 310130/2017-4 CNPq Productivity Research scholarship from 2018 to 2021; 317418/2021-1 CNPq Productivity Research scholarship from 2022 to 2026; (7) MCTI/CNPq partially financed the measurements, laboratory costs and scholarship for the period 2012–2013; (8) the Quadrature Climate Foundation (QCF)/World Meteorological Organization (WMO)—financed the measurements, laboratory costs and scholarship for the period 2023–2025; (9) the Imbuzeiro Institute—financed measurements, laboratory costs and scholarships for the period 2025–2026; CNPq 422354/2023-6—financing support for the PRODES program from 2023 to 2027. Clua—Climate and Land Use Alliance—financed IPAM activities and MapBiomas data used in the paper. The Article Processing Charge (APC) for the publication of this research was funded by the Coordenação de Aperfeiçoamento de Pessoal de Nível Superior - Brasil (CAPES) (ROR identifier: 00x0ma614).

Competing interests The authors declare no competing interests.

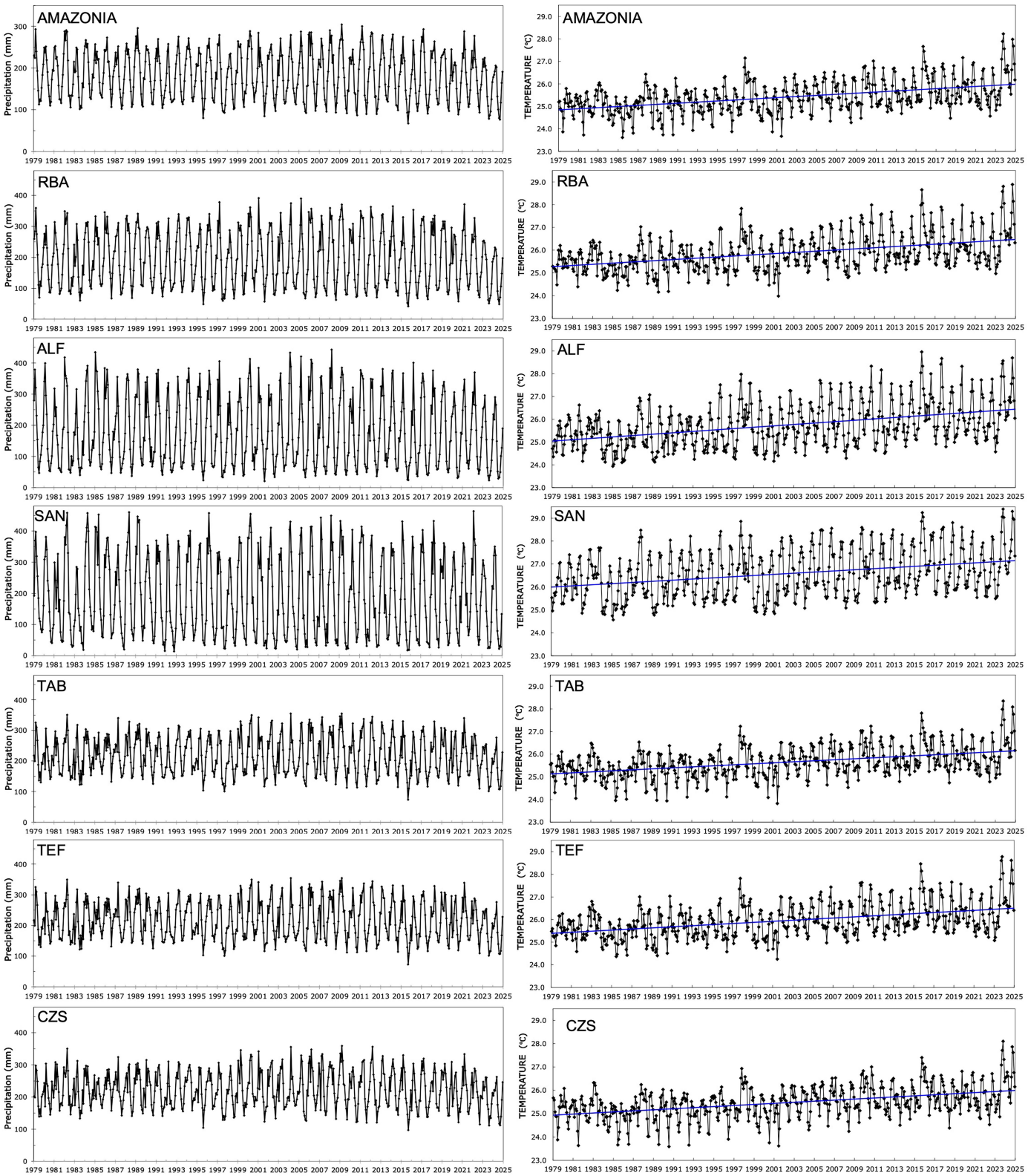
Additional information

Supplementary information The online version contains supplementary material available at https://doi.org/10.1038/s41586-026-11168-1.

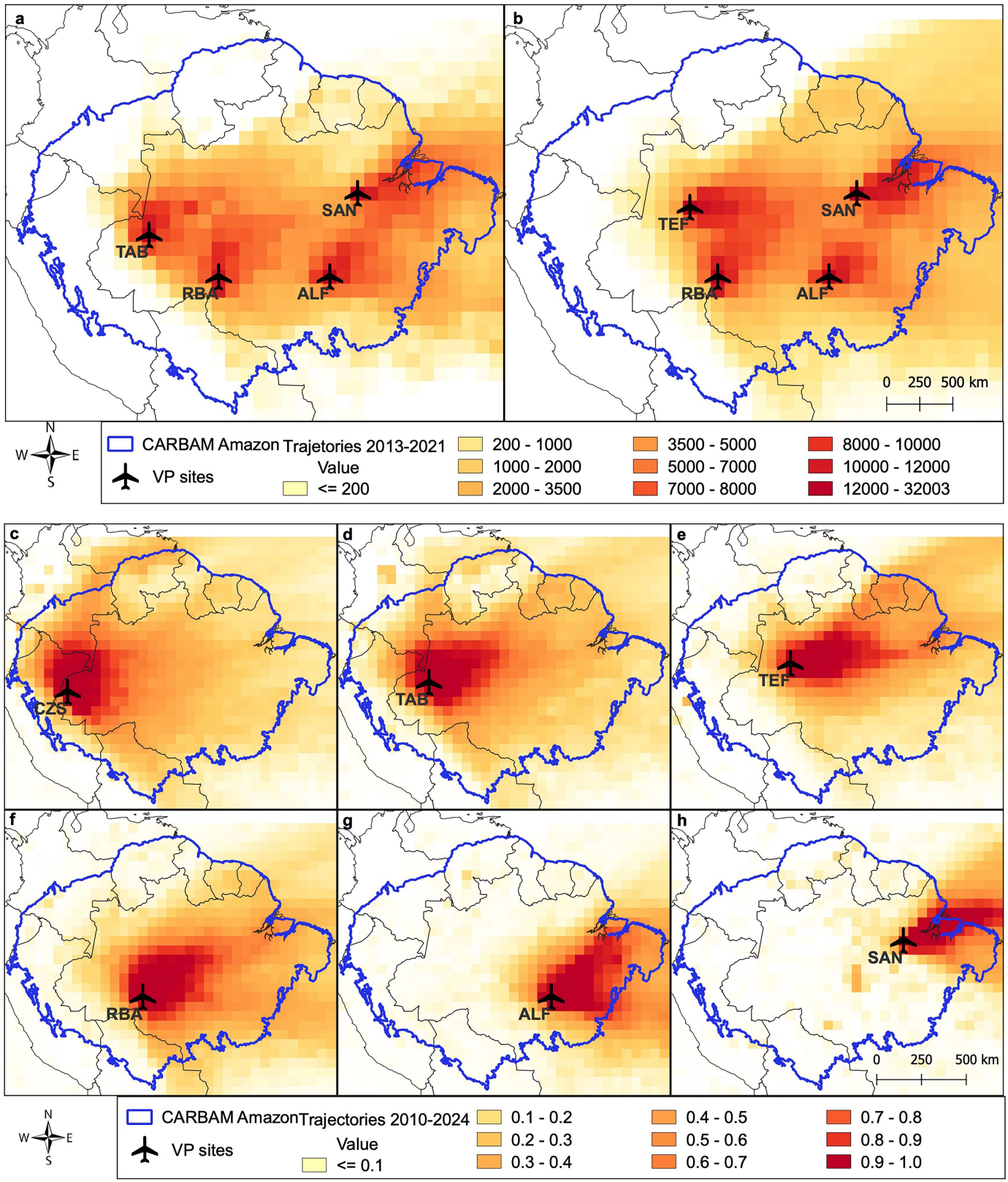
Correspondence and requests for materials should be addressed to Luciana V. Gatti.

Peer review information *Nature* thanks Albertus J. Dolman and the other, anonymous, reviewer(s) for their contribution to the peer review of this work. Peer reviewer reports are available.

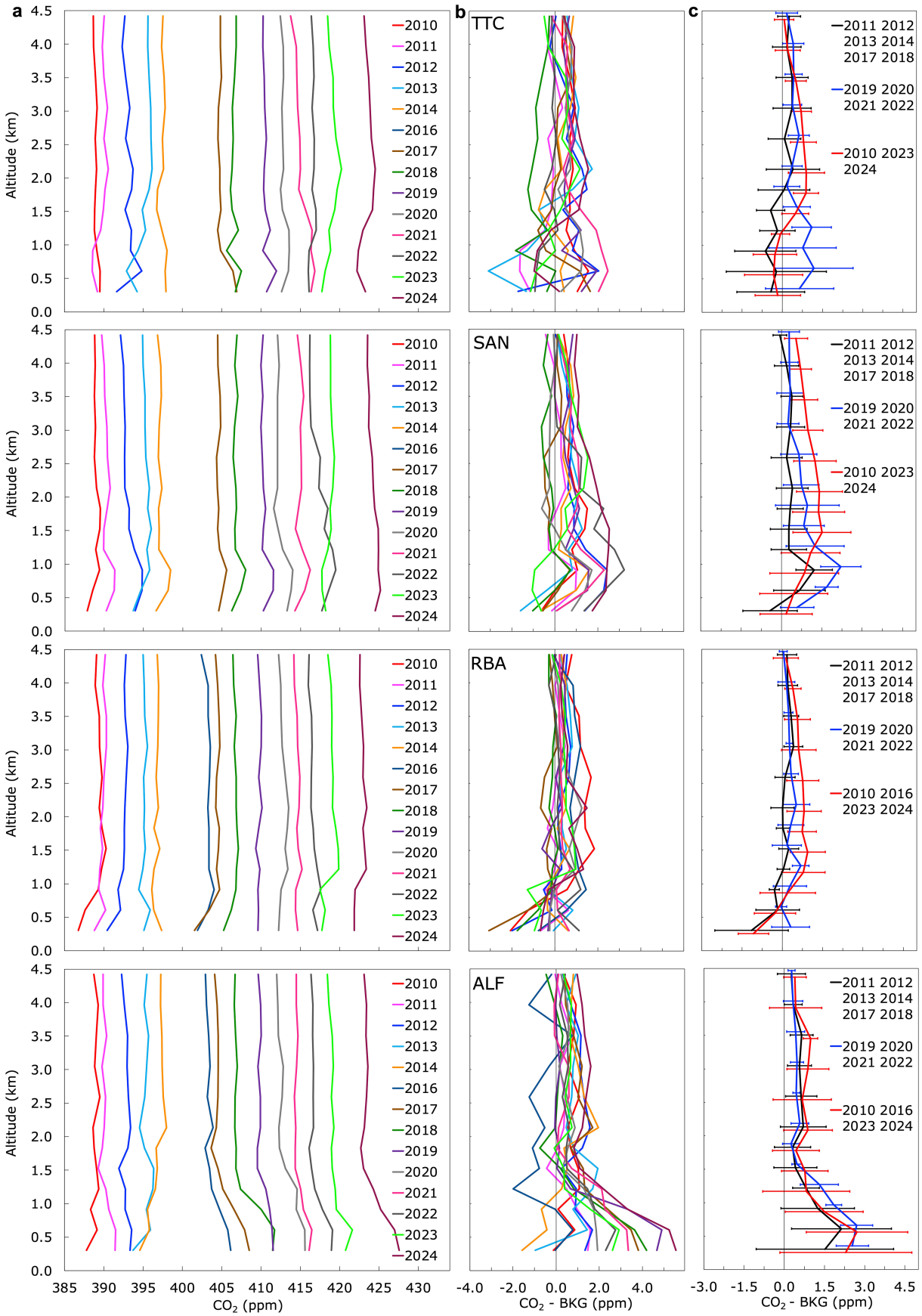
Reprints and permissions information is available at http://www.nature.com/reprints.



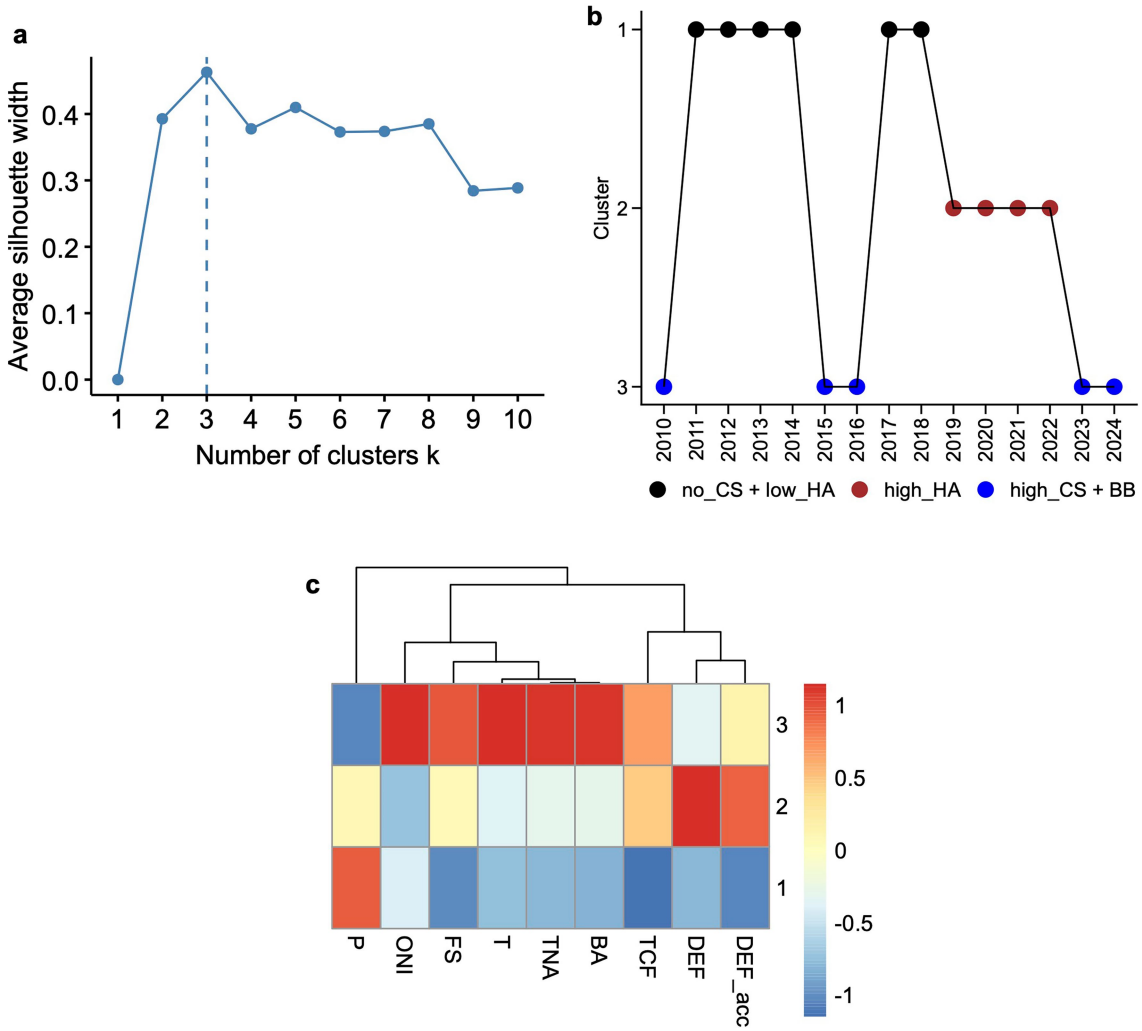
Extended Data Fig. 1 | 1979-2024 Amazonian precipitation and temperature. Amazonia monthly accumulated precipitation[54], monthly mean temperature[27] (Amazon mask area, Fig. 1 green line) for the period 1979 to 2024. Weighted monthly accumulated precipitation and weighted monthly mean temperature for the studied sites RBA, ALF, SAN, TAB, TEF, CZS (see regions in E. D. Fig. 1c–h), for the period 1979 to 2024 (see Methods), where it was calculated the weighted mean for each site using the region of influence from 2010–2024 as a spatial weighting function (see Methods).



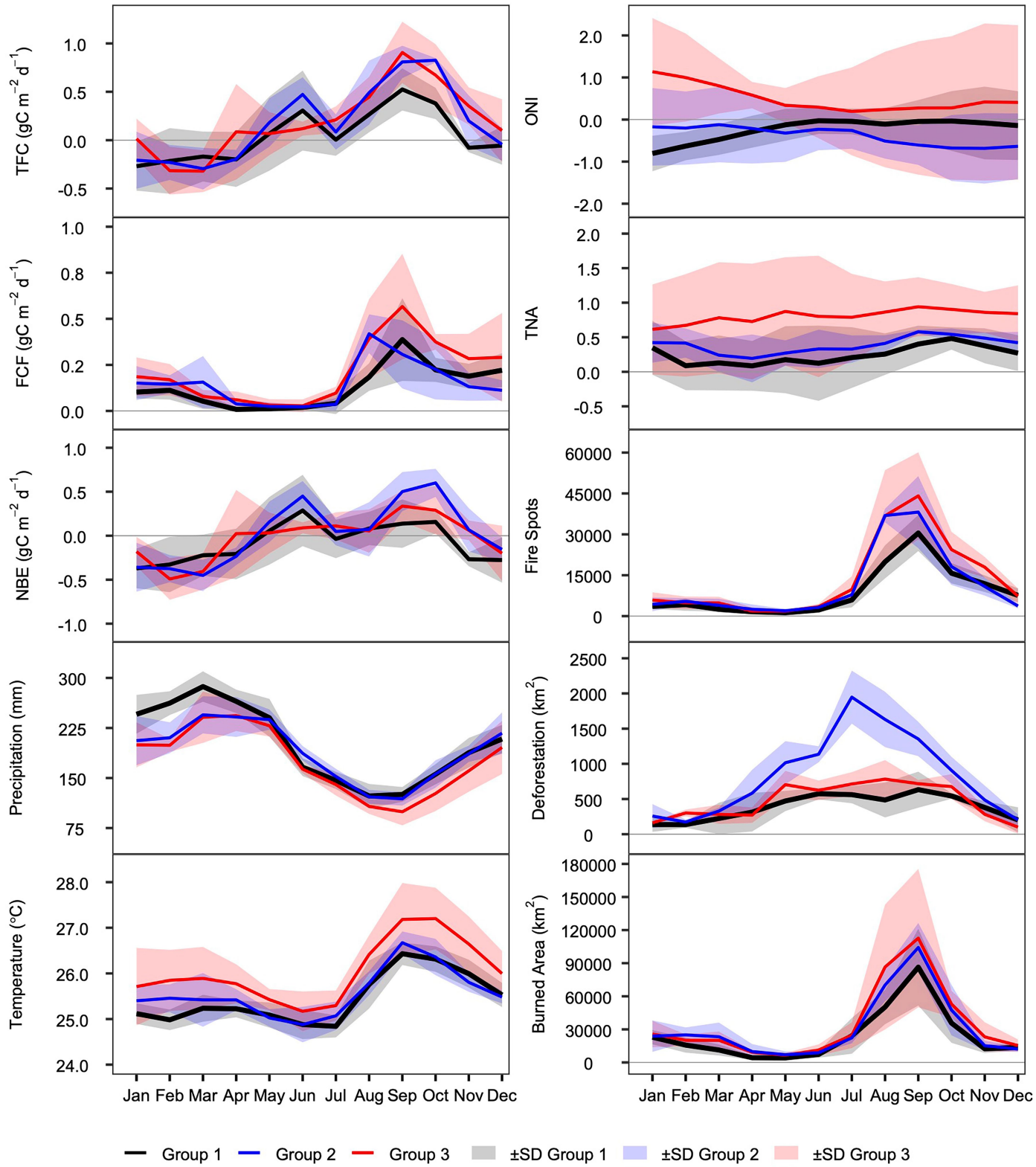
Extended Data Fig. 2 | Amazonia and VP sites regions of influence. a, Annual mean regions of influence, integrating RBA (f), ALF (g), SAN (h), and TAB (d) sites, based on back trajectories density along the years 2010-2012, calculated by the HYSPLIT trajectory model for each flask (sample height). **b**, Similar to a, but the northwest site between 2013 to 2021 was TEF (h). The regions of influence were based on the back trajectory density along the years, but with additional upgrade in our method described in the methods. **c**, **d**, **e**, **f**, **g**, and **h**, present the annual mean for each region of influence from the sites CZS, TAB, TEF, RBA, ALF, and SAN, respectively.



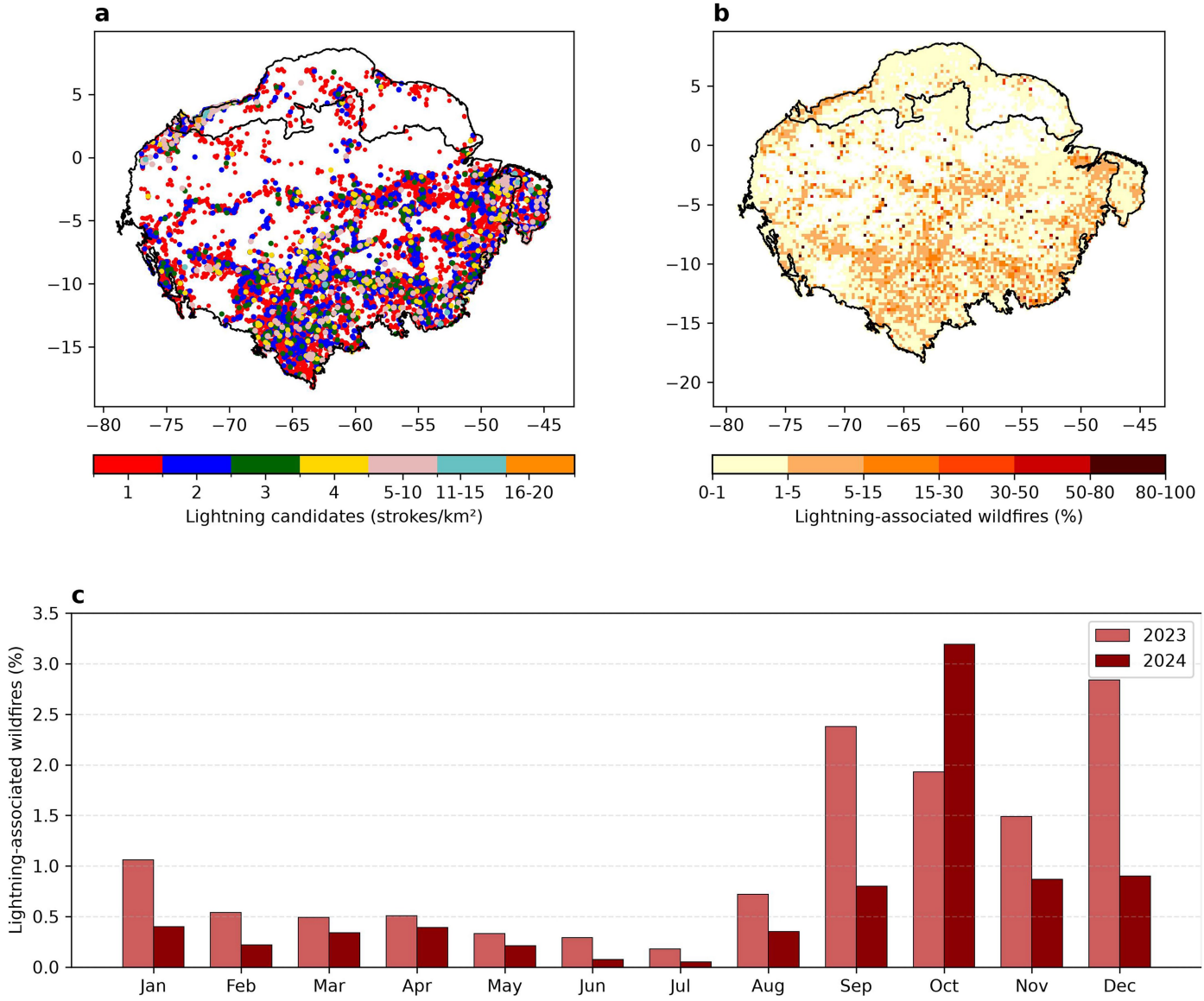
Extended Data Fig. 3 | Annual mean VP, and ΔVPs per site. a, Annual mean VPs for each site TAB_TEF_CZS, SAN, RBA, and ALF for the time series (2010–2024), constructed from the annual mean VP (see Methods). **b**, Annual mean ΔVPs for each site for the time series (2010–2024), constructed from the annual mean VP, where the background was subtracted from each height, each flask (see Methods). **c**, Annual mean ΔVPs according the three groups of years presented in the right legend.



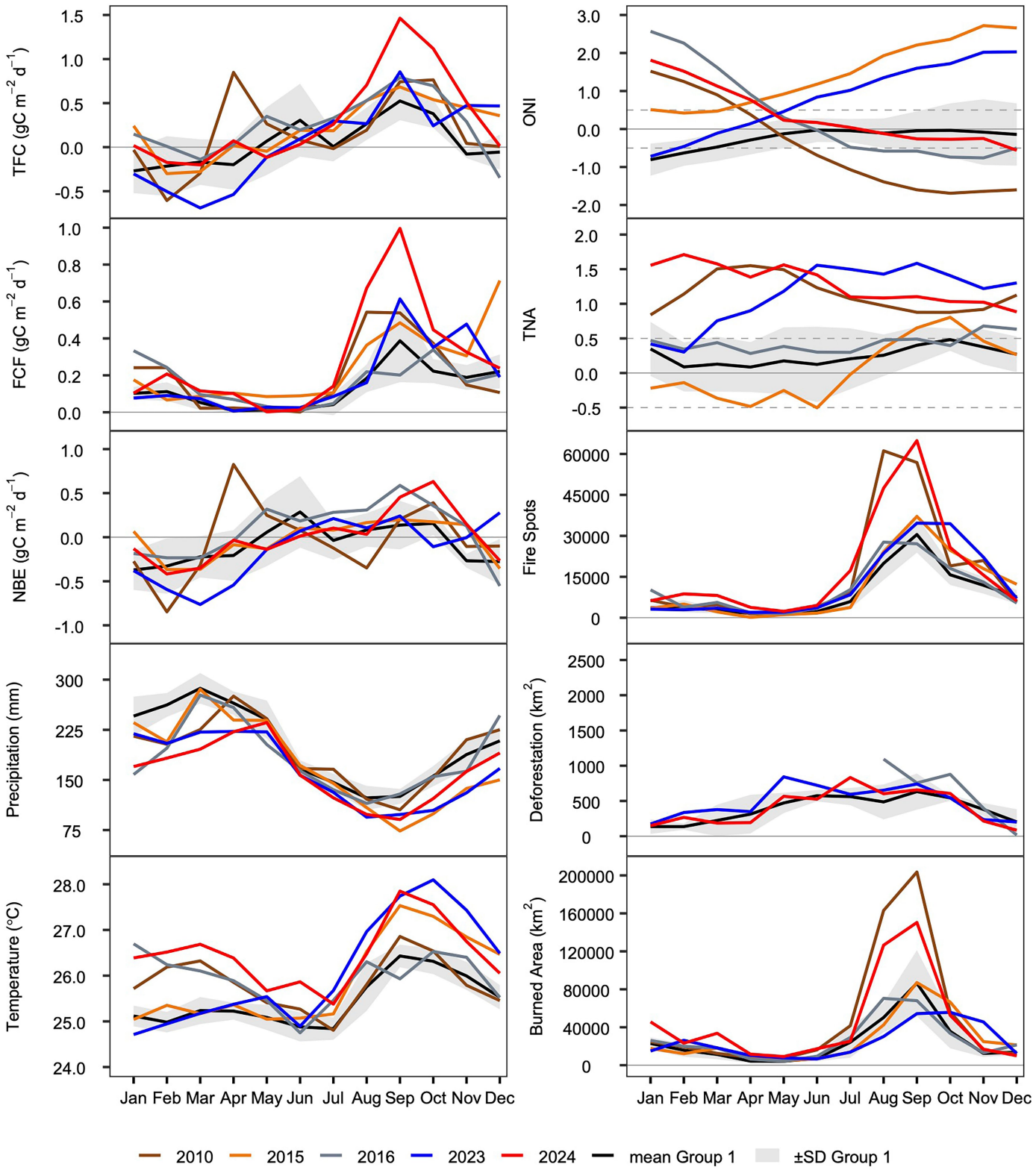
Extended Data Fig. 4 | K-means clustering in annual variables. **a**, Determination of the optimal number of clusters using the silhouette method, indicating k = 3 as the best partition. **b**, Distribution of observations across clusters derived from K-means clustering (k = 3), based on the selected variables (TCF, P, T, ONI, TNA, BA, FS, DEF and DEF_acc), highlighting separation in the multivariate space. **c**, Heatmap of standardised variables (z-scores), showing distinct multivariate signatures across clusters, with contrasting patterns in precipitation (P), temperature (T), fire spots (FS), burned area (BA), deforestation (DEF), accumulated deforestation (DEF_acc) and carbon emission (TCF).



Extended Data Fig. 5 | Seasonal Amazon C fluxes and drivers. Seasonal patterns of Amazonian carbon fluxes and drivers across the three groups. Seasonal monthly mean Amazonia Total C Flux (TCF), Fire C Flux (FCF) and NBE, and the group monthly mean for all drivers: precipitation[54], temperature[27], ONI[26], TNA[27], Fire Spots[63], Deforestation[61] (starting 2016), and burned area by MODIS[58] (Amazonia area, blue line Fig. 1).



Extended Data Fig. 6 | 2023 and 2024 Amazonia lightning-induced ignition. **a**, Spatial distribution of lightning candidates with 1 km spatial resolution. Label bar values indicate the number of candidate strokes per km2. **b**, Lightning-associated wildfires with 25 km resolution. **c**, Monthly distribution of lightning-associated wildfires for Amazonia, from 2023 to 2024.



Extended Data Fig. 7 | Group 3 Seasonal Amazon C fluxes and drivers. Seasonal behaviour of Amazon carbon fluxes and drivers for the years from Group 3 (2010, 2015, 2016, 2023, 2024). Seasonal monthly mean Amazonia Total C Flux, Fire C Flux and NBE, and the monthly mean for all drivers: precipitation[54], temperature[27], ONI[26], TNA[27], Fire Spots[63], Deforestation (starting 2016)[61], and burned area by MODIS[58], values corresponding to the Amazon mask area – blue line in the Fig. 1.

Extended Data Table 1 | Amazon temperature and precipitation over the past 40 and 46 years

Temperature	period	Accumulated deforestation (%)	Mean ASO		Annual Mean		Mean JFM	
			temperature increase (˚C)	annual growth rate (˚C/y)	temperature increase (˚C)	annual growth rate (˚C/y)	temperature increase (˚C)	annual growth rate (˚C/y)
Amazonia (6,700,798 km^2)	40 years (1979-2018)	19.5%	1.51 ± 0.17	0.038 ± 0.004	0.93 ± 0.13	0.023 ± 0.003	0.54 ± 0.24	0.014 ± 0.006
	46 years (1979-2024)	21.3%	1.81 ± 0.18	0.039 ± 0.004	1.13 ± 0.13	0.025 ± 0.003	0.69 ± 0.23	0.015 ± 0.005
ALF (1,698,179 km^2)	40 years (1979-2018)	31.1%	1.90 ± 0.18	0.048 ± 0.005	1.22 ± 0.17	0.031 ± 0.004	0.77 ± 0.22	0.019 ± 0.006
	46 years (1979-2024)	33.5%	2.19 ± 0.21	0.048 ± 0.005	1.37 ± 0.15	0.030 ± 0.003	0.90 ± 0.21	0.020 ± 0.005
SAN (709,846 km^2)	40 years (1979-2018)	35.7%	1.47 ± 0.19	0.037 ± 0.005	1.01 ± 0.18	0.025 ± 0.005	0.79 ± 0.28	0.020 ± 0.007
	46 years (1979-2024)	38.0%	1.61 ± 0.18	0.035 ± 0.004	1.10 ± 0.17	0.024 ± 0.004	0.80 ± 0.26	0.017 ± 0.006
RBA (3,637,777 km^2)	40 years (1979-2018)	16.8%	1.79 ± 0.21	0.045 ± 0.005	1.00 ± 0.14	0.025 ± 0.004	0.45 ± 0.23	0.011 ± 0.006
	46 years (1979-2024)	18.6%	2.05 ± 0.20	0.044 ± 0.004	1.17 ± 0.14	0.026 ± 0.003	0.56 ± 0.22	0.012 ± 0.005
TAB (3,724,750 km^2)	40 years (1979-2018)	8.9%	1.51 ± 0.15	0.038 ± 0.005	0.88 ± 0.13	0.022 ± 0.003	0.40 ± 0.24 (NS)	NS
	46 years (1979-2024)	10.1%	1.78 ± 0.19	0.039 ± 0.004	1.02 ± 0.13	0.022 ± 0.003	0.48 ± 0.23	0.010 ± 0.005
TEF (3,170,816 km^2)	40 years (1979-2018)	9.6%	1.61 ± 0.18	0.040 ± 0.005	0.94 ± 0.14	0.024 ± 0.004	0.49 ± 0.26 (NS)	NS
	46 years (1979-2024)	10.7%	1.89 ± 0.19	0.041 ± 0.004	1.09 ± 0.14	0.024 ± 0.003	0.59 ± 0.25	0.013 ± 0.005
CZS (3,662,874 km^2)	40 years (1979-2018)	9.1%	1.43 ± 0.18	0.036 ± 0.005	0.87 ± 0.13	0.022 ± 0.003	0.43 ± 0.24 (NS)	NS
	46 years (1979-2024)	10.4%	1.77 ± 0.19	0.038 ± 0.004	1.05 ± 0.13	0.023 ± 0.003	0.54 ± 0.13	0.012 ± 0.005
Precipitation	**period**	**Accumulated deforestation (km)**	**Precipitation reduction (mm)**	**annual reduction rate (mm/y)**	**Precipitation change (mm)**	**annual rate (mm/y)**	**Precipitation change (mm)**	**annual rate (mm/y)**
Amazonia (6,700,798 km^2)	40 years (1979-2018)	19.5%	↓ 64 ± 19 (17%)	↓ 1.6 ± 0.5	↓ 27 ± 69 (NS)	NS	↑ 44 ± 34 (NS)	NS
	46 years (1979-2024)	21.3%	↓ 83 ± 18 (20%)	↓ 1.8 ± 0.4	↓ 174 ± 69 (8%)	↓ 3.8 ± 1.5	↓ 42 ± 36 (NS)	NS
ALF (1,698,179 km^2)	40 years (1979-2018)	31.1%	↓ 54 ± 25 (20%)	↓ 1.4 ± 0.6	↓ 59 ± 122 (NS)	NS	↓ 16 ± 59 (NS)	NS
	46 years (1979-2024)	33.5%	↓ 70 ± 24 (26%)	↓ 1.5 ± 0.5	↓ 221 ± 120 (NS)	NS	↓ 90 ± 56 (NS)	NS
SAN (709,846 km^2)	40 years (1979-2018)	35.7%	↓ 67 ± 23 (34%)	↓ 1.7 ± 0.6	↓ 208 ± 167 (9%)	↓ 5.2 ± 4.2	↓ 103 ± 81 (11%)	↓ 2.6 ± 2.0
	46 years (1979-2024)	38.0%	↓ 77 ± 23 (37%)	↓ 1.7 ± 0.5	↓ 304 ± 150 (12%)	↓ 6.6 ± 3.3	↓ 142 ± 72 (14%)	↓ 3.1 ± 1.6
RBA (3,637,777 km^2)	40 years (1979-2018)	16.8%	↓ 84 ± 33 (20%)	↓ 2.1 ± 0.8	↑ 30 ± 104 (NS)	NS	↑ 80 ± 49 (NS)	NS
	46 years (1979-2024)	18.6%	↓ 95 ± 24 (25%)	↓ 2.1 ± 0.5	↓ 163 ± 110 (NS)	NS	↓ 26 ± 51 (NS)	NS
TAB (3,724,750 km^2)	40 years (1979-2018)	8.9%	↓ 77 ± 26 (16%)	↓ 1.9 ± 0.6	↑ 45 ± 95 (NS)	NS	↑ 102 ± 52 (14%)	↑ 2.5 ± 1.3
	46 years (1979-2024)	10.1%	↓ 95 ± 24 (19%)	↓ 2.0 ± 0.5	↓ 81 ± 91 (NS)	NS	↑ 26 ± 50 (NS)	NS
TEF (3,170,816 km^2)	40 years (1979-2018)	9.6%	↓ 72 ± 29 (20%)	↓ 1.8 ± 0.7	↓ 23 ± 125 (NS)	NS	↑ 59 ± 67 (NS)	NS
	46 years (1979-2024)	10.7%	↓ 76 ± 27 (20%)	↓ 1.7 ± 0.6	↓ 63 ± 108 (NS)	NS	↑ 9 ± 60 (NS)	NS
CZS (3,662,874 km^2)	40 years (1979-2018)	9.1%	↓ 67 ± 28 (13%)	↓ 1.5 ± 0.6	↑ 115 ± 87 (NS)	NS	↑ 152 ± 45 (21%)	↑ 3.3 ± 1.0
	46 years (1979-2024)	10.4%	↓ 87 ± 23 (16%)	↓ 1.9 ± 0.5	↓ 48 ± 83 (NS)	NS	↑ 47 ± 44 (NS)	NS

Observed trends for the periods 1979–2018, and 1979-2024, in annual mean temperature[27], and accumulated annual precipitation[54], for the whole Amazon, and the study sites RBA, ALF, SAN, TAB, TEF, CZS, using the region of influence from 2010–2024 as a spatial weighted method (see Methods). We also present trends for the wet (Jan, Feb, Mar) and dry (Aug, Sep, Oct) season peaks, as well as growth rates. Deforested areas for the sites were also calculated based on the weighted mean method. NS: non-significant.

Extended Data Table 2 | Annual Amazon and sites carbon flux and parameters

	Amazonia	2010	2011	2012	2013	2014	2015	2016	2017	2018	2019	2020	2021	2022	2023	2024
AMAZONIA (6.70 million km²)	TCF (PgC.y-1)	0.41	-0.01	0.32	0.28	0.16	0.52	0.59	0.07	-0.12	0.55	0.51	0.34	0.31	0.11	0.81
	NBE (PgC.y-1)	-0.07	-0.29	0.01	-0.02	-0.17	-0.08	0.19	-0.38	-0.36	0.07	0.12	0.08	-0.01	-0.33	-0.02
	FCF (PgC.y-1)	0.48	0.27	0.30	0.30	0.32	0.60	0.40	0.45	0.24	0.48	0.39	0.25	0.32	0.44	0.82
	VP - BKG	0.71	-0.05	0.48	0.31	0.31	0.00	0.57	0.01	-0.20	0.50	0.58	0.73	0.30	0.31	0.84
	P annuaL (mm)	2309	2516	2369	2482	2328	2092	2201	2394	2390	2423	2072	2414	2209	1973	1951
	P JFM (mm)	215	275	286	258	261	243	211	279	230	236	184	248	214	215	183
	P ASO (mm)	127	139	121	146	136	94	133	127	140	140	118	138	133	99	104
	T annual (°C)	25.8	25.4	25.4	25.4	25.5	25.9	25.9	25.7	25.4	25.6	25.8	25.4	25.4	26.1	26.5
	T JFM (°C)	26.1	24.9	24.8	25.4	25.1	25.2	26.3	25.2	25.3	25.5	25.9	25.1	25.2	24.9	26.5
	T ASO (°C)	26.4	26.2	26.3	25.7	26.1	27.1	26.3	26.6	26.1	26.2	26.5	26.4	26.1	27.6	27.3
	ONI	-0.49	-0.87	-0.14	-0.32	0.11	1.46	0.33	-0.20	0.01	0.48	-0.36	-0.72	-0.94	0.82	0.35
	TNA	1.13	0.59	0.36	0.31	-0.03	0.05	0.43	0.45	-0.20	0.20	0.52	0.39	0.44	1.13	1.29
	Fire Spot	195195	90999	118766	85933	106125	133519	128068	135694	104060	129016	149303	109431	160152	147581	210899
	BA (km2)	91523	34314	44164	36480	67180	101901	96414	98364	50186	74698	80559	41222	78511	83843	155413
	DEF (km2)	7270	5611	4849	6696	5909	7797	8527	7059	8208	12074	11300	13235	13712	8795	6671
	DEF_ac (km2)	686859	692470	697319	704015	709924	717721	726248	733307	741515	753589	764889	778124	791835	800630	807301
	DEF_ac (%)	18.1%	18.3%	18.4%	18.6%	18.7%	19.0%	19.2%	19.4%	19.6%	19.9%	20.2%	20.5%	20.9%	21.1%	21.3%

	ALF	2010	2011	2012	2013	2014	2015	2016	2017	2018	2019	2020	2021	2022	2023	2024
ALF (1.41 million km²)	TCF (PgC.y-1)	0.18	0.20	0.32	0.39	0.11	0.40	0.46	0.35	0.44	0.50	0.47	0.25	0.32	0.43	0.73
	NBE (PgC.y-1)	-0.07	0.05	0.12	0.25	-0.05	0.14	0.33	0.11	0.31	0.20	0.24	0.14	0.12	0.20	0.45
	FCF (PgC.y-1)	0.25	0.16	0.20	0.14	0.16	0.26	0.14	0.23	0.13	0.31	0.23	0.11	0.20	0.22	0.27
	VP - BKG	0.64	0.54	1.06	0.83	0.34		1.65	0.99	1.33	0.94	1.21	1.07	1.01	1.54	2.30
	P annuaL (mm)	1845	2214	1997	2223	2147	1691	1884	2065	2053	2224	1706	2030	1776	1541	1536
	P JFM (mm)	249	364	345	339	340	295	280	352	291	317	242	308	290	275	221
	P ASO (mm)	66	93	66	84	90	39	84	57	73	84	56	89	63	34	55
	T annual (°C)	26.5	25.7	25.8	26.0	26.1	26.6	26.6	26.5	26.1	26.3	26.0	25.8	25.9	26.6	26.9
	T JFM (°C)	26.0	25.0	24.7	25.4	25.0	25.3	26.2	25.4	25.3	25.4	25.8	25.3	25.3	25.1	26.4
	T ASO (°C)	27.7	27.0	27.2	27.0	27.2	28.3	27.3	28.1	27.4	27.5	27.0	27.2	27.3	28.2	28.0
	ONI	-0.49	-0.87	-0.14	-0.32	0.11	1.46	0.33	-0.20	0.01	0.48	-0.36	-0.72	-0.94	0.82	0.35
	TNA	1.13	0.59	0.36	0.31	-0.03	0.05	0.43	0.45	-0.20	0.20	0.52	0.39	0.44	1.13	1.29
	Fire Spot	49202	20174	24505	20313	24894	27443	23978	40523	18004	29733	22878	22137	29333	28003	54271
	BA (km2)	48135	14275	16795	13887	23095	41249	34341	51080	15843	27322	35174	12995	35558	27130	77683
	DEF (km2)	3880	2880	2201	2894	2347	3366	3599	2997	3286	5351	5364	5888	5466	3682	2736
	DEF_ac (km2)	348772	351651	353852	356746	359093	362459	366057	369054	372340	377691	383056	388944	394410	398092	400828
	DEF_ac (%)	29.1%	29.4%	29.6%	29.8%	30.0%	30.3%	30.6%	30.8%	31.1%	31.6%	32.0%	32.5%	32.9%	33.3%	33.5%

	RBA	2010	2011	2012	2013	2014	2015	2016	2017	2018	2019	2020	2021	2022	2023	2024
RBA (3.17 million km²)	TCF (PgC.y-1)	0.13	-0.02	0.00	0.08	0.00	0.18	0.20	-0.11	-0.06	0.02	0.16	-0.01	0.11	-0.01	0.16
	NBE (PgC.y-1)	-0.04	-0.11	-0.11	-0.04	-0.10	-0.09	0.01	-0.31	-0.13	-0.12	0.00	-0.11	0.00	-0.20	-0.21
	FCF (PgC.y-1)	0.17	0.08	0.11	0.12	0.10	0.27	0.20	0.20	0.08	0.14	0.16	0.10	0.11	0.19	0.36
	VP - BKG	0.59	0.02	0.01	0.35	0.26		0.70	-0.63	-0.35	0.01	0.37	0.33	0.39	0.11	0.40
	P annuaL (mm)	2113	2152	2159	2274	2127	1845	2045	2148	2081	2292	1685	2173	1753	1636	1542
	P JFM (mm)	258	304	326	300	311	288	267	309	252	279	181	296	228	245	188
	P ASO (mm)	95	105	80	100	92	46	105	83	92	104	78	108	92	54	60
	T annual (°C)	26.5	25.7	25.8	26.0	26.1	26.6	26.6	26.5	26.1	26.3	26.0	25.8	25.9	26.6	26.9
	T JFM (°C)	26.4	25.0	24.7	25.4	25.0	25.3	26.2	25.4	25.3	25.4	25.8	25.3	25.3	25.1	26.4
	T ASO (°C)	27.4	27.2	27.5	26.7	27.2	28.5	26.8	27.9	27.1	27.2	27.4	27.2	26.9	28.5	28.1
	ONI	-0.49	-0.87	-0.14	-0.32	0.11	1.46	0.33	-0.20	0.01	0.48	-0.36	-0.72	-0.94	0.82	0.35
	TNA	1.13	0.59	0.36	0.31	-0.03	0.05	0.43	0.45	-0.20	0.20	0.52	0.39	0.44	1.13	1.29
	Fire Spot	58435	24864	36126	22274	36975	39036	32811	49467	29854	39038	47390	34407	52430	40181	81580
	BA (km2)	36751	14275	16795	13887	23095	41249	34341	51080	15843	27322	35174	12995	35558	27130	77683
	DEF (km2)	3601	3245	2619	3688	3185	4508	4922	4496	4843	7067	6589	8111	8577	4909	3574
	DEF_ac (km2)	326750	329994	332614	336302	339487	343994	348917	353413	358256	365323	371913	380023	388601	393510	397084
	DEF_ac (%)	15.3%	15.5%	15.6%	15.8%	15.9%	16.1%	16.4%	16.6%	16.8%	17.1%	17.5%	17.8%	18.2%	18.5%	18.6%

	SAN	2010	2011	2012	2013	2014	2015	2016	2017	2018	2019	2020	2021	2022	2023	2024
SAN (0.63 million km²)	TCF (PgC.y-1)	0.43	0.24	1.01	0.39	0.27	0.67	0.38	0.05	-0.15	0.66	0.20	0.73	0.72	0.10	1.16
	NBE (PgC.y-1)	-0.18	-0.19	0.48	-0.08	-0.25	0.06	-0.03	-0.34	-0.38	0.25	-0.10	0.37	0.31	-0.29	0.37
	FCF (PgC.y-1)	0.61	0.43	0.53	0.47	0.52	0.60	0.41	0.39	0.23	0.41	0.31	0.35	0.41	0.39	0.78
	VP - BKG	0.67	0.19	1.15	0.42	0.50			-0.05	-0.24	0.82	0.31	0.96	1.51	0.25	1.86
	P annuaL (mm)	2179	2482	2147	2299	2134	1990	1907	2237	2338	2046	1851	2395	2350	1778	1793
	P JFM (mm)	224	355	351	265	306	280	236	368	261	198	175	290	319	274	226
	P ASO (mm)	64	64	44	73	55	23	46	38	45	49	53	83	57	24	37
	T annual (°C)	27.3	26.4	26.8	26.9	26.9	27.3	27.5	27.2	26.8	26.9	26.7	26.7	26.5	27.2	27.4
	T JFM (°C)	27.0	25.3	25.8	26.3	26.0	26.0	27.0	25.6	25.9	25.8	26.0	25.7	25.7	25.4	26.7
	T ASO (°C)	28.3	27.5	27.9	27.9	27.8	28.5	28.3	28.5	28.1	27.9	28.0	27.7	27.8	28.9	28.5
	ONI	-0.49	-0.87	-0.14	-0.32	0.11	1.46	0.33	-0.20	0.01	0.48	-0.36	-0.72	-0.94	0.82	0.35
	TNA	1.13	0.59	0.36	0.31	-0.03	0.05	0.43	0.45	-0.20	0.20	0.52	0.39	0.44	1.13	1.29
	Fire Spot	11030	7151	10245	7158	8243	10715	9022	12979	5610	6388	8302	5331	12859	11336	24411
	BA (km2)	7695	8856	8763	8278	12461	25583	20123	20918	8045	8114	11725	4943	14984	18414	35856
	DEF (km2)	2515	1583	977	1177	1021	1705	1532	1614	1393	2473	1989	2274	2237	1855	1590
	DEF_ac (km2)	186183	187767	188744	189921	190942	192647	194179	195793	197186	199659	201648	203922	206159	208014	209605
	DEF_ac (%)	33.7%	34.0%	34.2%	34.4%	34.6%	34.9%	35.2%	35.5%	35.7%	36.2%	36.5%	37.0%	37.4%	37.7%	38.0%

	TTC*	2010	2011	2012	2013	2014	2015	2016	2017	2018	2019	2020	2021	2022	2023	2024
TTC (2.83 million km²)	TCF (PgC.y-1)	0.16	-0.14	0.07	-0.02	0.10	0.11	0.14	0.04	-0.27	0.24	0.13	0.13	-0.08	-0.05	0.12
	NBE (PgC.y-1)	0.05	-0.20	0.02	-0.07	0.00	-0.04	0.04	-0.05	-0.34	0.07	0.06	0.08	-0.14	-0.17	-0.02
	FCF (PgC.y-1)	0.11	0.06	0.05	0.06	0.09	0.15	0.09	0.09	0.08	0.16	0.07	0.05	0.06	0.12	0.14
	VP - BKG	0.79	-0.54	0.57	-0.15	0.26			0.29	-0.76	0.80	0.70	1.17	-0.32	0.00	0.47
	P annuaL (mm)	2220	2332	2307	2388	2059	1904	2048	2156	2114	2240	2021	2354	2064	1986	1870
	P JFM (mm)	227	262	295	237	216	219	180	249	172	175	128	218	188	187	168
	P ASO (mm)	114	129	108	127	113	65	122	104	101	123	109	140	134	111	87
	T annual (°C)	26.3	26.0	26.0	26.2	26.3	26.7	26.7	26.4	26.2	26.3	26.4	26.0	25.7	26.2	26.8
	T JFM (°C)	26.5	25.4	25.2	25.8	25.6	25.6	26.7	25.4	25.8	26.0	26.4	25.4	25.5	25.1	26.7
	T ASO (°C)	26.9	26.8	27.0	26.8	27.1	28.3	27.1	27.6	27.2	27.0	27.2	26.9	26.4	27.8	27.8
	ONI	-0.49	-0.87	-0.14	-0.32	0.11	1.46	0.33	-0.20	0.01	0.48	-0.36	-0.72	-0.94	0.82	0.35
	TNA	1.13	0.59	0.36	0.31	-0.03	0.05	0.43	0.45	-0.20	0.20	0.52	0.39	0.44	1.13	1.29
	Fire Spot	49767	18480	24087	13299	15961	17703	19198	25740	18096	20734	22271	14126	49139	22980	67487
	BA (km2)	21285	8081	9424	6758	12159	20885	23134	22097	10906	12887	15809	7562	19201	16743	56496
	DEF (km2)	1986	1702	1308	1620	1511	2135	2204	2073	2169	3704	3179	3862	4792	2596	2013
	DEF_ac (km2)*	155530	157232	158540	165899	167410	169545	171749	173822	175992	179696	182875	186738	170643	173238	175251
	DEF_ac (%)	8.1%	8.2%	8.2%	9.1%	9.2%	9.3%	9.4%	9.5%	9.6%	9.8%	10.0%	10.2%	10.1%	10.3%	10.4%

*TTC: 2010-2012 TAB; 2013-2021 TEF; 2022-2024 CZS

Results for all years presenting the carbon fluxes and the studied parameters: Total (TCF), Fire (FCF), and NBE, annual mean ΔVP, annual accumulated precipitation (P)[54], monthly mean precipitation for the months Jan-Mar (P_{JFM}), and for Aug-Oct (P_{ASO}), annual mean temperature (T)[27], monthly mean temperature for the months Jan-Mar (T_{JFM}), and for Aug-Oct (T_{ASO}), ONI (Oceanic Niño Index)[26], TNA (Tropical Northern Atlantic Ocean anomaly (71-00) index[27], Fire Spots (FS)[63], Burned Area (BA)[25], annual deforestation (DEF)[21], accumulated Deforested (DEF_ac and in %) (see Methods).

Extended Data Table 3 | Carbon fluxes and studied parameters by groups

a

	GROUP 1 (no_CS + low_HA)							
Variables	**2011**	**2012**	**2013**	**2014**	**2017**	**2018**	**Mean**	**STDev**
TCF (PgC.y-1)	-0.01	0.32	0.28	0.16	0.07	-0.12	**0.11**	**0.17**
NBE (PgC.y-1)	-0.29	0.01	-0.02	-0.17	-0.38	-0.36	**-0.20**	**0.17**
FCF (PgC.y-1)	0.27	0.30	0.30	0.32	0.45	0.24	**0.32**	**0.07**
VP - BKG	-0.05	0.48	0.31	0.31	0.01	-0.20	**0.14**	**0.26**
P annuaL (mm)	2516	2369	2482	2328	2394	2390	**2413**	**72**
P JFM (mm)	275	286	258	261	279	230	**265**	**20**
P ASO (mm)	139	121	146	136	127	140	**135**	**9**
T annual (°C)	25.4	25.4	25.4	25.5	25.7	25.4	**25.4**	**0.1**
T JFM (°C)	24.9	24.8	25.4	25.1	25.2	25.3	**25.1**	**0.2**
T ASO (°C)	26.2	26.3	25.7	26.1	26.6	26.1	**26.2**	**0.3**
ONI	-0.87	-0.14	-0.32	0.11	-0.20	0.01	**-0.23**	**0.35**
TNA	0.59	0.36	0.31	-0.03	0.45	-0.20	**0.25**	**0.30**
Fire Spot	90999	118766	85933	106125	135694	104060	**106930**	**18281**
BA (km2)	34314	44164	36480	67180	98364	50186	**55115**	**24249**
DEF_an (km2)	5611	4849	6696	5909	7059	8208	**6389**	**1188**
DEF_ac (km2)	692470	697319	704015	709924	733307	741515	**713091**	**19915**
DEF_ac (%)	18.3%	18.4%	18.6%	18.7%	19.4%	19.6%	**18.8%**	**0.5%**

b

	GROUP 2 (high_HA)					
Variables	**2019**	**2020**	**2021**	**2022**	**Mean**	**STDev**
TCF (PgC.y-1)	0.55	0.51	0.34	0.31	**0.43**	**0.12**
NBE (PgC.y-1)	0.07	0.12	0.08	-0.01	**0.07**	**0.05**
FCF (PgC.y-1)	0.48	0.39	0.25	0.32	**0.36**	**0.10**
VP - BKG	0.50	0.58	0.73	0.30	**0.53**	**0.18**
P annuaL (mm)	2423	2072	2414	2209	**2280**	**170**
P JFM (mm)	236	184	248	214	**220**	**28**
P ASO (mm)	140	118	138	133	**132**	**10**
T annual (°C)	25.5	25.9	25.1	25.2	**25.4**	**0.4**
T JFM (°C)	25.5	25.9	25.1	25.2	**25.4**	**0.4**
T ASO (°C)	26.2	26.5	26.4	26.1	**26.3**	**0.2**
ONI	0.48	-0.36	-0.72	-0.94	**-0.39**	**0.62**
TNA	0.20	0.52	0.39	0.44	**0.39**	**0.13**
Fire Spot	129016	149303	109431	160152	**136976**	**22444**
BA (km2)	74698	80559	41222	78511	**68747**	**18510**
DEF_an (km2)	12074	11300	13235	13712	**12580**	**1096**
DEF_ac (km2)	753589	764889	778124	791835	**772109**	**16537**
DEF_ac (%)	19.9%	20.2%	20.5%	20.9%	**20.4%**	**0.4%**

c

	GROUP 3 (High_CS + BB)						
Variables	**2010**	**2015**	**2016**	**2023**	**2024**	**Mean**	**STDev**
TCF (PgC.y-1)	0.41	0.52	0.59	0.11	0.81	**0.49**	**0.26**
NBE (PgC.y-1)	-0.07	-0.08	0.19	-0.33	-0.02	**-0.06**	**0.19**
FCF (PgC.y-1)	0.48	0.60	0.40	0.44	0.82	**0.55**	**0.17**
VP - BKG	0.71		0.57	0.31	0.84	**0.61**	**0.23**
P annuaL (mm)	2309	2092	2201	1973	1951	**2105**	**152**
P JFM (mm)	215	243	211	215	183	**213**	**21**
P ASO (mm)	127	94	133	99	104	**111**	**17**
T annual (°C)	25.8	25.2	26.3	24.9	26.5	**25.8**	**0.7**
T JFM (°C)	26.1	25.2	26.3	24.9	26.5	**25.8**	**0.7**
T ASO (°C)	26.4	27.1	26.3	27.6	27.3	**26.9**	**0.6**
ONI	-0.49	1.46	0.33	0.82	0.35	**0.50**	**0.72**
TNA	1.13	0.05	0.43	1.13	1.29	**0.81**	**0.54**
Fire Spot	195195	133519	128068	147581	210899	**163052**	**37610**
BA (km2)	91523	101901	96414	83843	155413	**105819**	**28508**
DEF_an (km2)	7270	7797	8527	8795	6671	**7812**	**877**
DEF_ac (km2)	686859	717721	726248	800630	807301	**747752**	**53419**
DEF_ac (%)	18.1%	19.0%	19.2%	21.1%	21.3%	**19.7%**	**1.4%**

Group 1 represents years without climatic stress and low human activity. Group 2 represents high human activity and low climatic stress, and Group 3 represents high climatic stress associated with biomass burning. Items **a**, **b**, and **c** correspond to the Groups 1, 2 and 3, respectively, and present the annual and mean group carbon fluxes and the studied parameters. Total C Flux (TCF), Fire C Flux (FCF), NBE, annual mean ΔVP, precipitation (P)[54], Jan-Mar mean precipitation (P_{JFM}), and for Aug-Oct (P_{ASO}), temperature (T)[27], Jan-Mar mean temperature (T_{JFM}), and for Aug-Oct (T_{ASO}), ONI[26], TNA[27], fire spots (FS)[63], burned area (BA)[25], annual deforestation (DEF)[21], and accumulated deforested (DEF_acc and in %).